Journal of Integrative Agriculture 2026, 25(9): 3673–3691

Available online at ScienceDirect

Journal of Integrative Agriculture

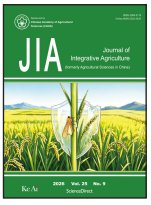

RESEARCH ARTICLE

Antagonism and convergence of *MiCOL14B*-GQ and *MiCOL14B*-JH in mango (*Mangifera indica*) flowering and abiotic stress

Junjie Zhong, Ruoyan Li, Yuan Liu, Shuquan Chen, Huibao Wen, Teng Tang, Cong Luo[#], Xinhua He[#]

State Key Laboratory for Conservation and Utilization of Subtropical Agro-Bioresources/Guangxi Key Laboratory for Agro-Environment and Agro-Product Safety/National Demonstration Center for Experimental Plant Science Education, College of Agriculture, Guangxi University, Nanning 530004, China

Highlights

- *MiCOL14B*-GQ delays flowering whereas *MiCOL14B*-JH promotes flowering in transgenic *Arabidopsis*.
- MiCOL14B-GQ represses the transcription activity of the *MiFT*, whereas MiCOL14B-JH promotes it.
- Both *MiCOL14B*-GQ and *MiCOL14B*-JH confer increased resistance to salt and drought stress in plants.

Abstract

The *CONSTANS/CONSTANS-LIKE* (CO/*COL*) gene family plays important roles in plants flowering and stress response. In this study, two variants of the *MiCOL14B* gene were identified from two different mango cultivars; they were designated as *MiCOL14B*-GQ and *MiCOL14B*-JH, which exhibited significant differences in sequence and B-box domain. Both genes were expressed in various tissues of mango, localized in the nucleus, and responsive to drought and salt stress. In transgenic *Arabidopsis thaliana*, *MiCOL14B*-GQ delayed flowering, while *MiCOL14B*-JH promoted flowering. This phenotypic divergence stemmed from their molecular regulatory specificity. Yeast one-hybrid (Y1H) and dual-luciferase reporter assays demonstrated that both variants directly bind to the promoters of florigen genes (*MiFT*s), with MiCOL14B-GQ repressing their transcription and MiCOL14B-JH enhancing it. Altered expression levels of *MiFT*s in the roots of transgenic mango further validated this mechanism. Moreover, both *MiCOL14B*-GQ and *MiCOL14B*-JH improved stress tolerance under drought and salt conditions in transgenic *A. thaliana* as well as in transgenic mango roots. These variants significantly increased stress tolerance by increasing proline (Pro) content and superoxide dismutase (SOD) activity, while reducing malondialdehyde (MDA) and hydrogen peroxide (H_2O_2) accumulation. Yeast two-hybrid (Y2H) and bimolecular fluorescence complementation (BiFC) assays revealed that MiCOL14B-GQ and MiCOL14B-JH interact with several stress-related proteins. This study demonstrates for the first time the functional effects of sequence variation in the *MiCOL14B* gene on flowering and stress responses, providing valuable genetic resources for mango molecular breeding.

Keywords: mango, *MiCOL14B*, flowering regulation, abiotic stress, protein interaction

1. Introduction

Plants regulate flowering time to adapt to changing environments and ensure successful reproduction under optimal conditions, a process critical for their survival and propagation (Niu *et al.* 2024). Flowering is a complex developmental transition governed by the interplay of genetic programs and environmental cues, enabling plants to synchronise floral initiation with external signals and internal growth status. Multiple regulatory pathways have been identified, including photoperiod, vernalization, gibberellin (GA), age, nutrient, autonomous, and ambient temperature pathways (Okamuro *et al.* 1997; Blazquez *et al.* 1998; Mutasa and Hedden 2009; Wu *et al.* 2009; Srikanth and Schmid 2011; Wullschleger and Weston 2012). Among these, the photoperiod pathway, which is mediated by photoreceptors that perceive day-length changes, orchestrates the *CO*/*COL*-*FT* regulatory module (Endo *et al.* 2013) and serves as a central mechanism for integrating environmental signals to trigger floral initiation.

CO/*COL* genes act as central regulators in photoperiod signalling, thereby integrating light and circadian cues to

Received 22 April 2025; Received in revised form 21 November 2025; Accepted 29 December 2025; Available online 13 January 2026
[#]Correspondence Cong Luo, E-mail: 22003luocong@163.com; Xinhua He, E-mail: hexh@gxu.edu.cn

doi: 10.1016/j.jia.2026.01.012

activate *FT* expression. The *FT* gene encodes florigen, which is synthesized in leaves, translocated to the shoot apical meristem (SAM) and then activates flowering-related genes to induce floral meristem differentiation (Putterill *et al.* 1995; Wigge *et al.* 2005; Corbesier *et al.* 2007). Structurally, CO/COL proteins harbor two conserved domains: an N-terminal B-box zinc finger domain that mediates protein-protein interactions and a C-terminal CCT (CONSTANS, CONSTANS-like, and TIMING OF CAB EXPRESSION 1) domain that is responsible for nuclear localization and DNA binding (Robson *et al.* 2001). Mutations in the B-box domain disrupt such interactions and compromise COL protein function (Lagercrantz and Axelsson 2000). The *COL* genes can be divided into three subfamilies on the basis of the number and arrangement of B-box and CCT domains. Specifically, subfamily B1 is characterized by two B-box domains and a single CCT domain; subfamily B2 contains one B-box domain, one CCT domain, and a zinc finger-like motif; and subfamily B3 comprises one B-box domain and one CCT domain.

Genomic analyses have revealed that the *CO*/*COL* gene family is widely distributed across both dicotyledonous and monocotyledonous plant lineages, a feature characterised by high evolutionary conservation of structural domains and pronounced functional diversification. These genes play pivotal roles in regulating flowering time, stress responses, and multiple aspects of plant development. Despite the structural conservation of their B-box and CCT domains, there is substantial functional divergence among *COL* family members: certain homologues promote floral transition, whereas others repress it, a phenomenon that likely reflects adaptive evolution to distinct environmental niches. Remarkable progress has been made in clarifying the roles of *CO/COL* genes in regulating photoperiodic flowering. In *Arabidopsis thaliana*, *CO* was among the first identified key regulators of flowering, driving floral transition under long-day (LD) conditions by activating *FT* expression (Putterill *et al.* 1995). Subsequent cloning of *HEADING DATE 1* (*HD1*) in rice revealed its high sequence homology and functional equivalence to *AtCO*, thus demonstrating the conserved roles of these genes in photoperiodic flowering across distantly related species (Yano *et al.* 2000; Tamaki *et al.* 2007; Nemoto *et al.* 2016). The functional diversification of *COL* homologues across other taxa is evident, in that *VcCO3* in blueberry (*Vaccinium corymbosum*) promotes floral bud induction (Feng *et al.* 2025), whereas in moso bamboo (*Phyllostachys edulis*), *PeCOL13α* delays heading (Ma *et al.* 2024), and heterologous overexpression of *COL1* and *COL3* from *Pinus tabuliformis* in *A. thaliana* delays flowering (Yang *et al.* 2024), in pitaya (*Hylocereus polyrhizus*), FLOWERING BHLHs (HpFBH3) may promote flowering through transcriptional activation of *HpCO7* (Cai *et al.* 2025). Collectively, these findings underscore their conserved yet context-dependent roles in plant reproductive development. Beyond regulating flowering, compelling evidence from cross-species functional studies has established that *COL* genes are pivotal players in plant responses to abiotic stresses. For example, in banana (*Musa acuminata*), *MaCOL1* integrates fruit ripening pathways with chilling stress tolerance (Chen *et al.* 2012); *BnCOL2* in rapeseed (*Brassica napus*) compromises drought resistance when overexpressed in *A. thaliana* (Liu *et al.* 2020a); *ThCOL2* in *Tamarix hispida* increases salt tolerance in tobacco (Lei *et al.* 2021); *MdCOL9* in apple (*Malus domestica*) improves drought resistance (Chen *et al.* 2022); and *GmCOL1a* in soybean (*Glycine max*) increases tolerance to salt and drought stresses (Xu *et al.* 2023). These findings underscore the versatile roles of *COL* genes in integrating developmental programs and environmental adaptation, establishing them as critical nodes in mediating plant stress resilience and adaptive fitness.

Mango (*Mangifera indica* L.), a pivotal export crop in tropical and subtropical regions is highly valued for its distinct flavour profile and high nutritional value. It is widely cultivated in southern China. However, during the flowering stage, mango trees are often subjected to low temperatures and rainy conditions, which induce abnormalities in the meiosis of pollen mother cells. These abnormalities impair pollen viability and fertilization efficiency, triggering extensive fruit abscission that severely reduces mango yield and causes considerable economic losses (Huang *et al.* 2010). In addition, the growth and development of mango are frequently constrained by various abiotic stresses, including drought and salt stress. Most mango cultivars are highly sensitive to soil and water salinization, especially at the seedling stage. This sensitivity results in reduced seedling vigour, necrosis at leaf tips and margins, leaf curling, and in severe instances, the death of entire plants. Drought stress adversely affects mango productivity by triggering the accumulation of reactive oxygen species, thus inducing oxidative stress. Furthermore, the reduced uptake of water and nutrients under drought stress further inhibits mango seedling growth (Bajpai *et al.* 2017; Deivasigamani *et al.* 2018). Therefore, precisely regulating the flowering period and enhancing mango tolerance to abiotic stresses represent key breakthroughs for improving mango yield stability and fruit quality. In our previous research, 31 *COL* genes were identified in the mango genome, and functional characterization of several *MiCOL* genes was conducted *via* transgenic *A. thaliana* assays (Liu *et al.* 2022b). For example, the overexpression of *MiCO* in *A. thaliana* delayed flowering (Liu *et al.* 2020b). The overexpression of *MiCOL7A* and *MiCOL7B* led to delayed floral transition, whereas *MiCOL6* overexpression promoted early flowering. These transgenic *A. thaliana* lines presented increased SOD activity and Pro content, reduced MDA accumulation, and improved survival rates under drought and salt stress (Liu *et al.* 2024). Mechanistic studies indicated that these *MiCOL* genes may regulate flowering by modulating the expression of *FT*, a key gene encoding florigen in plants. In mango, *MiFT* has been demonstrated to strongly promote flowering (Li *et al.* 2024). Notably, *MiFT* expression was significantly altered in *MiCO*-overexpressing transgenic plants, consistent with the conserved role of the *CO-FT* signalling module in flowering regulation, as established in *A. thaliana*.

This study identifies two allelic variants of the *MiCOL14B* gene, designated as *MiCOL14B*-GQ and *MiCOL14B*-JH, from the cultivars ‘Guiqi’ and ‘Jinhuang’, respectively. These two variants exhibit distinct protein domain architectures:

MiCOL14B-GQ contains two B-box domains and one CCT domain, whereas *MiCOL14B*-JH possesses only a single CCT domain. In mango production, 'Guiqi' is a mid-maturing cultivar, whereas 'Jinhuang' is an early-maturing cultivar. Both cultivars share favourable agronomic traits, including strong adaptability, tolerance to infertile soil, and ease of cultivation (Chen 2000, 2002). These findings suggest that the allelic variations in *MiCOL14B* may concurrently regulate flowering time and stress responses. Thus, we employed transgenic approaches, expression correlation analyses, and stress physiological experiments to elucidate the regulatory mechanisms through which these structural variations modulate flowering time and stress tolerance. The results not only clarify the functional differentiation patterns of *COL* genes in tropical fruit trees but also provide candidate targets for mango molecular design and facilitating the development of novel cultivars with adjustable flowering periods and enhanced stress resistance.

2. Materials and methods

2.1. Plant materials

Five-year-old *M. indica* cvs. 'Guiqi' and 'Jinhuang' were planted in the mango garden of Guangxi University (108.33°E, 22.84°N, Nanning, Guangxi, China). On 15 March, 2024, stem, leaf, bud, and floral tissues were collected for tissue-specific expression analysis. For temporal expression profiling, fully expanded leaves were sampled monthly from November 2024 to March 2025. To characterize gene expression under abiotic stress, two-year-old grafted mango seedlings were subjected to treatments with 300 mmol L^{-1} NaCl (salt stress) or 30% (w/v) polyethylene glycol 6000 (PEG 6000, simulated drought). Samples were collected at 0, 12, 24, 36, 48, 60, and 72 h post-treatment. Immediately after collection, all samples had been flash-frozen in liquid nitrogen and stored at –80°C until subsequent analysis. Wild-type (*A. thaliana* Columbia ecotype) and transgenic plant lines were grown in a controlled environment growth chamber under standardized long-day (LD) conditions, with a 16 h light /8 h dark photoperiod at 22±1°C.

2.2. Identification and sequence analysis of *MiCOL14B*

Two allelic variants of *MiCOL14B* were isolated from the transcriptome datasets of 'Guiqi' and 'Jinhuang' mango cultivars (unpublished data), and their sequences were validated by Sanger sequencing. These variants were designated as *MiCOL14B*-GQ and *MiCOL14B*-JH, respectively. The cloning primers used were *MiCOL14B*-GQ F/R and *MiCOL14B*-JH F/R. The PCR products were subsequently cloned into the pMD18-T vector and subjected to Sanger sequencing. The amino acid sequences, molecular weights (MW), and isoelectric points (pIs) of MiCOL14B proteins were analysed using BioXM 2.7.1 software. *Cis*-regulatory elements in the 2-kb promoter regions upstream of the two variants were predicted using the PlantCARE database (https://bioinformatics.psb.ugent.be/webtools/plantcare/html/) and visualized with TBtools. Related CO/COL protein sequences were retrieved using BLAST (http://www.ncbi.nlm.nih.gov/BLAST/), and a multiple sequence alignment was performed using DNAMAN 7 software. A neighbor-joining phylogenetic tree of *MiCOL14B* and *COL* family genes was generated with MEGA 6.06 (with 1,000 bootstrap replicates). The subcellular localization of MiCOL14B variants was computationally predicted with Plant-mPLoc (http://www.csbio.sjtu.e du.cn/bioinf/plant-multi).

2.3. RNA extraction and qRT-PCR

Total RNA was extracted from mango tissues using the PureLink Plant RNA Kit (Magen, Guangzhou, China), and first-strand cDNA was synthesized using the M-MLV Reverse Transcriptase Kit (TaKaRa, Dalian, China) according to the manufacturer's protocol, using *MiActin1* as the reference gene (Luo *et al.* 2013; Li *et al.* 2025). qRT-PCR was performed using the SYBR *PreMix Ex Taq* II Kit (TaKaRa) on an ABI 7500 Real-Time PCR System (Applied Biosystems, CA, USA). The reaction setup and thermal cycling conditions followed the manufacturers' recommendations. The gene-specific qRT-PCR primers are listed in Appendix A. Relative gene expression was calculated using the $2^{-\Delta\Delta CT}$ method (Livak and Schmittgen 2001). All experiments included three biological replicates, each with three technical replicates.

2.4. Vector construction and generation of transgenic plants

The full-length coding sequences (CDS) of *MiCOL14B*-GQ and *MiCOL14B*-JH were cloned into the pBI121 vector and the recombinant constructs were introduced into *Agrobacterium tumefaciens* strain EHA105. *Arabidopsis thaliana* (Col-0) plants were transformed using the floral dip method. Homozygous T_3 transgenic lines were obtained by selection on medium containing 50 mg L^{-1} kanamycin and confirmed by PCR. From these, three independent transgenic lines for each variant that exhibited high transgene expression levels, as determined by qRT-PCR, were selected for subsequent experiments. The expression levels in these lines were significantly higher than in the wild-type plants (Student's *t*-test, $P<0.05$). The primer sequences for the reference gene *AtActin2* used in qRT-PCR are provided in Appendix A.

The pBI121-*MiCOL14B*-GQ and pBI121-*MiCOL14B*-JH plasmids were introduced into *Agrobacterium rhizogenes* strain K599 using the freeze-thaw method. The the 'cut-dip-budding' delivery system was employed for transformation (Cao *et al.* 2023). Briefly, under non-sterile conditions, the root-shoot junctions of mango seedlings were wounded and the wounded sites were inoculated with *A. rhizogenes* strain K599. The inoculated plants were cultured in a vermiculite-based substrate at 28°C and 70%–80% relative humidity. After 4–6 weeks, hairy roots emerged at the inoculated sites. The transgenic nature of the hairy roots was verified by PCR and sequencing, confirming the correct integration and orientation of the transgene. Transgene expression in the positive hairy roots was further quantified by qRT-PCR.

2.5. Phenotypic analysis of flowering and endogenous gene expression in transgenic *A. thaliana*

T_3-generation transgenic *A. thaliana* plants were cultivated

under LD conditions. Flowering time was recorded as the number of days from sowing to the first flower opening. WT and empty vector (pBI121) transformed plants serving as negative controls to evaluate the phenotypic effects of transgene expression. Prior to flowering, whole plant tissues were harvested for total RNA extraction, followed by first-strand cDNA synthesis. qRT-PCR was performed to analyse the relative expression levels of key flowering regulators: *AtFT*, *SUPPRESSOR OF OVEREXPRESSION OF CONSTANS 1* (*AtSOC1*), and *APETALA 1* (*AtAP1*). The gene-specific primers, designed for specific amplification of coding sequences, are listed in Appendix A. All qRT-PCR reactions were performed with three technical replicates, and expression levels were normalized to the reference gene *AtActin2*.

2.6. Phenotypic analysis of stress responses and measurement of physiological indicators and endogenous gene expression in transgenic *A. thaliana*

To assess the abiotic stress tolerance, transgenic *A. thaliana* lines were phenotypically and physiologically analyzed at specific developmental stages. For root growth assays, T_3 transgenic and WT seedlings were germinated and vertically grown on 1/2 Murashige and Skoog (MS) media supplemented with NaCl (0, 100, or 200 mmol L^{-1}) or mannitol (0, 300, or 400 mmol L^{-1}) for 5 d under standard conditions. Root lengths were measured for 10 seedlings per replicate, with three biological replicates per treatment. For late-stage stress tolerance evaluation, 7-d-old WT and transgenic seedlings were transplanted into square pots (5 seedlings per pot, three replicates) and acclimated under normal conditions for 1 week. The plants were then subjected to three treatment regimes: regular watering (control), irrigation with 300 mmol L^{-1} NaCl every 3 d for 14 d (salt stress), and complete water deprivation for 12 d (drought stress). Survival rates were recorded 7 d after re-watering (for drought) or after the final NaCl application (for salt stress), based on the recovery of plants that produced new green leaves.

For physiological characterization, 3-week-old transgenic and WT *A. thaliana* plants were subjected to foliar spraying with water (control), 10% (w/v) PEG 6000, or 150 mmol L^{-1} NaCl solution. Three hours after treatment, rosette leaves were harvested and individually incubated in nitrotetrazolium blue chloride (NBT, 0.5 mg mL^{-1}, pH 7.0) for 3 h to detect superoxide anion ($O_2^{\cdot-}$) accumulation, Evans blue (EB, 2.5% w/v) for 30 min to assess plasma membrane integrity, and 3,3′-diaminobenzidine (DAB, 1.0 mg mL^{-1}, pH 3.8) for 8 h to visualize H_2O_2 deposition. Chlorophyll was removed by immersion in 95% ethanol heated to 65°C for 2 h to clear the background staining. Additionally, leaf samples were collected 2 d after treatment to quantify the Pro content, MDA concentration, SOD activity, and H_2O_2 levels *via* commercial assay kits (Solarbio, Beijing, China) according to the manufacturer's protocols, with three biological replicates per treatment.

To investigate the molecular mechanisms underlying stress responses, qRT-PCR was performed to analyse the expression of abiotic stress-responsive genes in WT and transgenic *A. thaliana*. One-month-old plants were treated with 150 mmol L^{-1} NaCl or 10% (w/v) PEG 6000 to simulate salt and drought stress, respectively. Entire aerial tissues were harvested. The expression profiles of six stress-related genes were examined: three salt-responsive genes *Salt Overly Sensitive 1* (*AtSOS1*), Na^+/H^+ *Antiporter 1* (*AtNHX1*), and *Dehydration Responsive Element Binding Protein 2A* (*AtDREB2A*) and three drought-responsive genes *Kinesin-Like Protein 1* (*AtKIN1*), *Cold-Regulated 15A* (*AtCOR15A*), and *Responsive To Desiccation 29A* (*AtRD29A*). The gene-specific primers used are listed in Appendix A. Each sample was analysed with three biological replicates to ensure data reproducibility.

2.7. Endogenous gene expression analysis and stress physiological index measurement in transgenic mango hairy roots

To characterise the physiological functions of the transgenic mango plants, we conducted gene expression and physiological analyses on 8–12-week-old transgenic hairy roots. First, qRT-PCR was used to quantify the expression levels of flowering-related genes, including *MiFT1a1* and *MiFT1b*. For preliminary exploration of drought and salt stress responses, hairy roots were immersed in 300 mmol L^{-1} NaCl or 30% (w/v) PEG 6000 solutions for 48 h. After treatment, hairy roots were harvested to measure key physiological indices: Pro as an indicator of cellular osmoregulation, MDA to assess membrane lipid peroxidation, SOD activity as a marker of antioxidant capacity, and H_2O_2 levels to evaluate oxidative stress severity (Grace, Suzhou, China). These measurements provided a comprehensive assessment of stress-induced physiological alterations in the hairy roots of transgenic mango plants. The gene-specific sequences of primers used are listed in Appendix A, and each sample was analysed with three biological replicates to ensure data reliability.

2.8. Yeast one-hybrid (Y1H)

The interaction between MiCOL14B-GQ/JH and the CORE1/CORE2 elements in the *MiFT*s promoter was assessed using the Y1H system. Briefly, partial promoter fragments of *MiFT*s were cloned into the pAbAi vector to generate the bait plasmid pAbAi-MiFTs. Separately, the coding sequences for *MiCOL14B*-GQ and *MiCOL14B*-JH were cloned into the pGADT7 vector to construct the prey plasmids, pGADT7-MiCOL14B-GQ and pGADT7-MiCOL14B-JH, respectively. All constructs were verified by sequencing. The pAbAi-MiFTs bait plasmid was transformed into Y1HGold competent cells (provided by Vidal Biotechnology, Shanghai, China) to create the Y1HGold yeast competent cells to generate the reporter strain. Subsequently, the pGADT7-MiCOL14B-GQ and pGADT7-MiCOL14B-JH prey plasmids were independently introduced into this strain. The transformed yeasts were plated on SD/–Leu medium supplemented with aureobasidin A (AbA) and incubated in the dark at 30°C for 3–5 d to monitor the growth of positive colonies. Empty pAbAi and pGADT7 vectors were used as negative controls to confirm interaction specificity, while known interacting pairs served as positive controls. All experiments were performed in triplicate

with independent biological replicates, and statistical analysis was conducted to assess the significance of the observed interactions.

2.9. Dual-luciferase assay

To characterize the regulatory role of MiCOL14B-GQ/JH in *MiFT*s promoter activity, we performed a dual-luciferase assay in *Nicotiana benthamiana* leaves. The *MiFTs* promoter was cloned into the pGreenII0800-LUC vector to generate the reporter construct, while the coding sequences of *MiCOL14B*-GQ and *MiCOL14B*-JH were inserted into the pGreenII-62-SK vector to create the effector plasmids, pGreenII-62-SK-MiCOL14B-GQ and pGreenII-62-SK-MiCOL14B-JH, respectively. These recombinant plasmids were separately transformed into *A. tumefaciens* strain GV3101. Positive colonies, verified by PCR, were inoculated into LB liquid media containing the appropriate antibiotics and cultured at 28°C with shaking until the OD_{600} reached 0.8. For infiltration, the bacterial cultures carrying the effector plasmids (pGreenII-62-SK-MiCOL14B-GQ or pGreenII-62-SK-MiCOL14B-JH) were mixed with the culture containing the reporter plasmid (pGreenII0800-LUC-PMiFTs) at a 9:1 ratio (effector:reporter). The mixture was then diluted to a final OD_{600}=0.8 using an infiltration buffer (10 mmol L^{-1} MES, 10 mmol L^{-1} $MgCl_2$, 150 μmol L^{-1} acetosyringone, pH 5.6). The bacterial suspensions were infiltrated into the abaxial side of *N. benthamiana* leaves, with at least five leaves per treatment. The infiltrated tobacco plants were then incubated in a growth chamber at 22°C in the dark for 48–72 h. Finally, the LUC signals were imaged using a plant *in vivo* imaging system.

2.10. Transcriptional activity analysis

To assess the transcriptional activation activity of MiCOL14B-GQ and MiCOL14B-JH, their full-length CDS and middle region (MR)-deleted variants were PCR-amplified and cloned into the pGBKT7 vector, generating BD-MiCOL14B-GQ, BD-MiCOL14B-JH, BD-MiCOL14B-GQ-ΔMR, and BD-MiCOL14B-JH-ΔMR constructs. These constructs were subsequently transformed into Y2HGold yeast cells. The transformed yeasts were cultured on SD/–Trp, SD/–Trp/X-α-gal, or SD/–Trp/X-α-gal/AbA media to screen for transactivation activity. The empty pGBKT7 vector was used as a negative control to monitor any autonomous activation by the bait proteins.

2.11. Yeast two-hybrid (Y2H)

To identify proteins interacting with MiCOL14B-GQ and MiCOL14B-JH, the BD-MiCOL14B-GQ-ΔMR and BD-MiCOL14B-JH-ΔMR constructs were used as baits in a Y2H screening. Prior to the screening, we confirmed that neither the bait constructs nor the prey proteins exhibited autonomous activation. The prey proteins tested included MiWRKY12a, MiWRKY12A, MiWRKY12B, MiWRKY13A, MiWRKY13B, and four abiotic stress-related proteins: RING-TYPE ZINC FINGER PROTEIN 34 (MiRZFP34), NAC DOMAIN CONTAINING PROTEIN 7 (MiNAC7), MYB30-INTERACTING E3 LIGASE 1 (MiEIEL1), and PROTEIN PHOSPHATASE 2C 39A (MiPP2C39A). For the interaction assay, plasmids encoding these prey proteins were transformed into Y187 yeast cells, which were then mated with Y2HGold cells harboring the bait constructs. The diploid yeast cells were first plated on SD/–Leu/–Trp (DDO) medium to select for successful mating and then transferred to stricter SD/–Ade/–His/–Leu/–Trp/AbA (QDO/A) medium for 4–5 d to assess protein-protein interactions. All experiments included at least three independent replicates to ensure reliability and reproducibility.

2.12. Subcellular localization analysis

To determine the subcellular localization of MiCOL14B-GQ and MiCOL14B-JH, their full-length cDNA sequences were amplified and cloned in-frame into the pBI221-EGFP vector, with the fusion constructs placed under the control of the cauliflower mosaic virus (CaMV) 35S promoter. The resulting 35S:MiCOL14B-GQ-EGFP and 35S:MiCOL14B-JH-EGFP plasmids were transformed into *A. tumefaciens* GV3101 cells, which were then used to transiently transform epidermal cells of *Allium cepa* (onion) scales. The subcellular localization of the EGFP-tagged fusion proteins was visualized *via* a confocal laser scanning microscope (TCS-SP8MP, Leica, Germany). The empty pBI221-EGFP vector, which expresses free EGFP without the target protein, served as a control to confirm nonspecific fluorescence. Nuclei were counterstained with 4′,6-diamidino-2-phenylindole (DAPI, 1 μg mL^{-1}) to facilitate subcellular compartment localization, and images were acquired under identical excitation/emission settings to ensure comparability.

2.13. Bimolecular fluorescence complementation (BiFC)

To perform BiFC assays, the target genes *MiCOL14B*-GQ and *MiCOL14B*-JH were cloned into the pUC-SPYNE and pUC-SPYCE vectors, respectively. The resulting recombinant plasmids were subsequently transformed into *A. tumefaciens* GV3101 competent cells to obtain bacterial suspensions containing the target plasmids. These suspensions were mixed at a 1:1 ratio according to the experimental design and infiltrated into the inner epidermal cells of onion (*Allium cepa*) bulbs. The YFP fluorescence signals were observed under a confocal laser scanning microscope to verify protein-protein interactions. The empty pUC-SPYNE and pUC-SPYCE vectors were used as negative controls to exclude nonspecific fluorescence signals.

2.14. Statistical analysis

Error bars in the figures represent the standard errors (SE). Statistical analyses were performed using SPSS software (version 22.0). Significance was assessed with Student's *t*-test, with $P<0.05$ indicated by single asterisks (*) and $P<0.01$ by double asterisks (**). Bar charts were generated with GraphPad Prism (version 7.0).

3. Results

3.1. Analysis of the *MiCOL14B*-GQ and *MiCOL14B*-JH sequences

Bioinformatics analysis showed that the *MiCOL14B*-

GQ gene spans 1,421 bp of genomic DNA and contains a 1,089 bp cDNA encoding a 362-amino acid protein. In contrast, *MiCOL14B*-JH comprises 3,568 bp of genomic DNA and a 1,134 bp cDNA that encodes a 377-amino acid protein. Structural annotation revealed that *MiCOL14B*-GQ consists of two introns and three exons, while *MiCOL14B*-JH contains four introns and five exons (Fig. 1-A). BLAST homology searches against the NCBI database indicated that *MiCOL14B*-GQ contains two conserved N-terminal B-box domains and a C-terminal CCT domain, whereas *MiCOL14B*-JH contains only the CCT domain (Fig. 1-B). Subcellular localization predictions using the Plant-mPLoc server suggested that both proteins are localized to the nucleus. Physicochemical property analysis *via* BioXM 2.7.1 software revealed that MiCOL14B-GQ has a molecular weight of 40.69 kDa and a theoretical pI of 6.01, whereas MiCOL14B-JH has a molecular weight of 41.45 kDa and a theoretical pI of 4.48.

To explore the regulatory potential of *MiCOL14B*-GQ and *MiCOL14B*-JH, the 2,000 bp genomic sequences upstream of their respective start codons were analysed for *cis*-acting elements using the PlantCARE bioinformatics tool, and the results were visualized *via* TBtools software. This analysis revealed numerous light-responsive elements in both promoter regions, suggesting a likely role in photoperiod-mediated flowering regulation. Additionally, hormone-responsive, stress-responsive, and circadian-responsive elements were identified, along with binding motifs for transcription factor families including RELATED TO ABI3/VP1 1 (RAV1), WRKY, MYB, and INDUCER OF CBF EXPRESSION (ICE) (Fig. 1-C). These findings indicate that *MiCOL14B*-GQ and *MiCOL14B*-JH may participate in hormone signalling pathways, stress adaptation, and transcriptional regulatory networks that coordinate developmental and environmental responses.

To elucidate the evolutionary relationships of the *COL* gene family across plant species, a phylogenetic tree was constructed using the neighbor-joining method, incorporating sequences from a diverse set of species with an emphasis on horticultural crops, including *Citrus sinensis*, *Pistacia vera*, *Durio zibethinus*, *Mangifera indica*, *Malus domestica*, *Vitis vinifera*, *Solanum lycopersicum*, and *Oryza sativa*. Phylogenetic

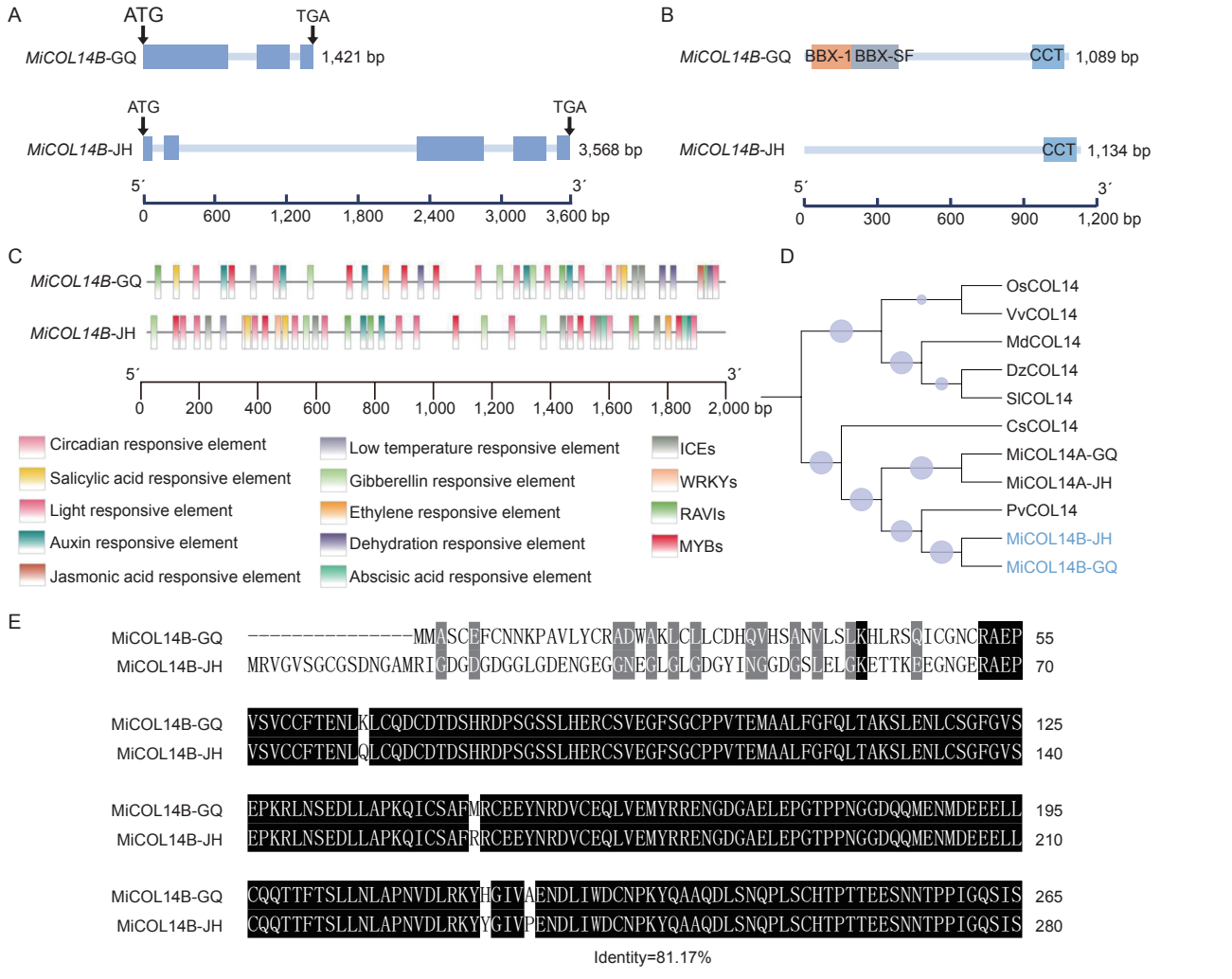

Fig. 1 Sequence and phylogenetic analysis of *MiCOL14B*-GQ and *MiCOL14B*-JH. A, gene structure: boxes represent exons, and lines represent introns. B, conservation analysis. C, promoter *cis*-element analysis. D, phylogenetic tree with other COL protein, the circle size represents genetic distance. E, sequence alignment.

analysis results show that MiCOL14B-GQ and MiCOL14B-JH belong to the same evolutionary clade, indicating that they have a close phylogenetic relationship and relatively high sequence conservation (Fig. 1-D). The sequence similarity between MiCOL14B-GQ and MiCOL14B-JH was 81.17% (Fig. 1-E).

3.2. Expression patterns of *MiCOL14B*-GQ and *MiCOL14B*-JH

qRT-PCR was used to analyze the expression profiles of *MiCOL14B*-GQ and *MiCOL14B*-JH in mango plants. Tissue-specific expression analysis revealed that both genes were expressed in all examined tissues, including the leaves, stems, and buds of non-flowering branches, as well as the leaves, stems, and flowers of flowering branches. Notably, *MiCOL14B*-GQ had the highest expression levels in the leaves of non-flowering branches, with the second-highest expression in the flowers of flowering branches (Fig. 2-A). In contrast, *MiCOL14B*-JH had the highest expression in the leaves of non-flowering branches, followed by buds (Fig. 2-B).

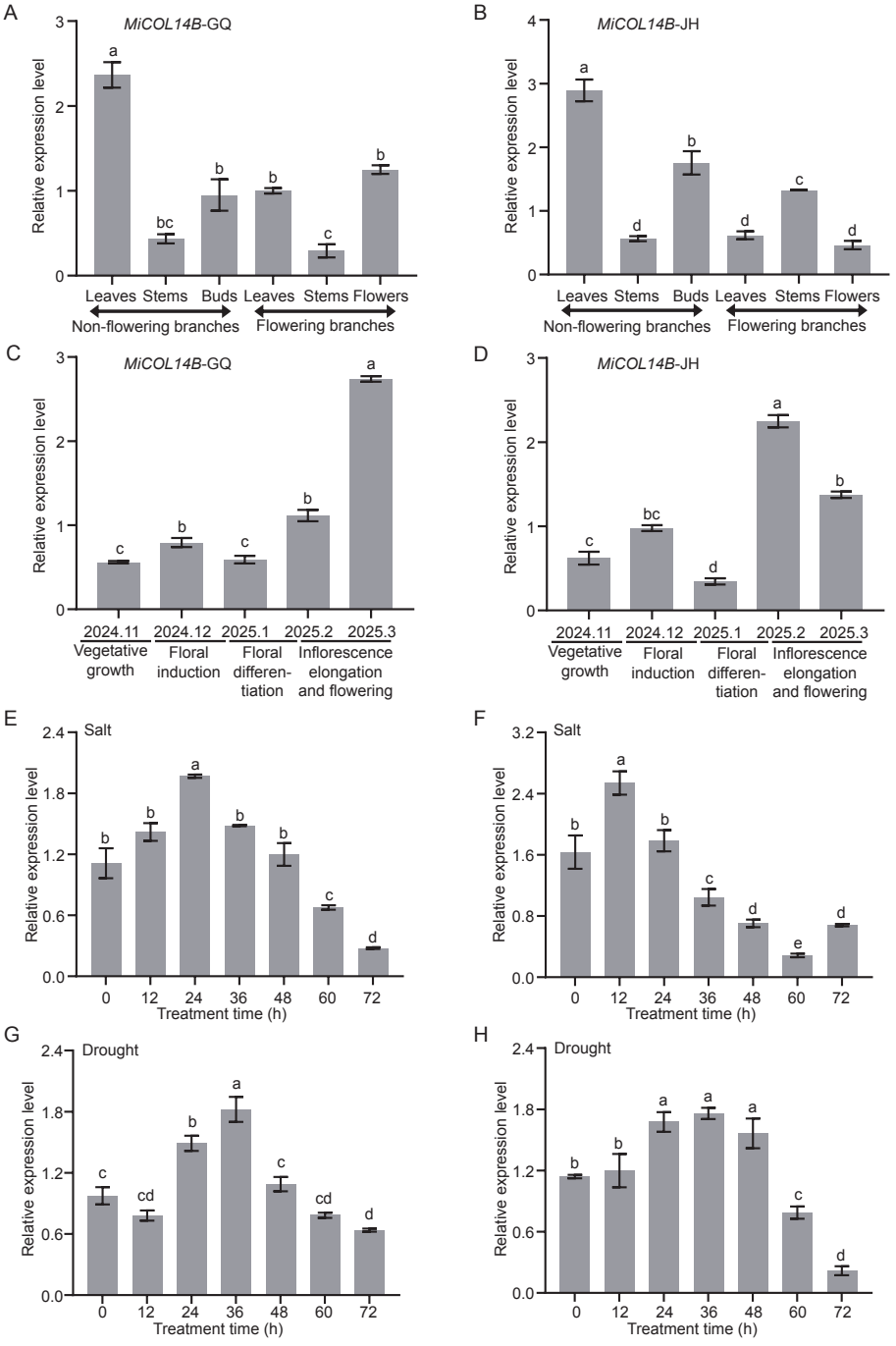

Fig. 2 Expression patterns of *MiCOL14B*-GQ and *MiCOL14B*-JH. A and B, tissue-specific expression patterns across non-flowering and flowering branches. C and D, temporal expression analysis. E–H, dynamic expression profiles of *MiCOL14B*-GQ and *MiCOL14B*-JH under salt (NaCl) and drought (PEG 6000) stress over a 72-h time course. Distinct letters attached to the data indicate significant differences among treatments (P<0.05).

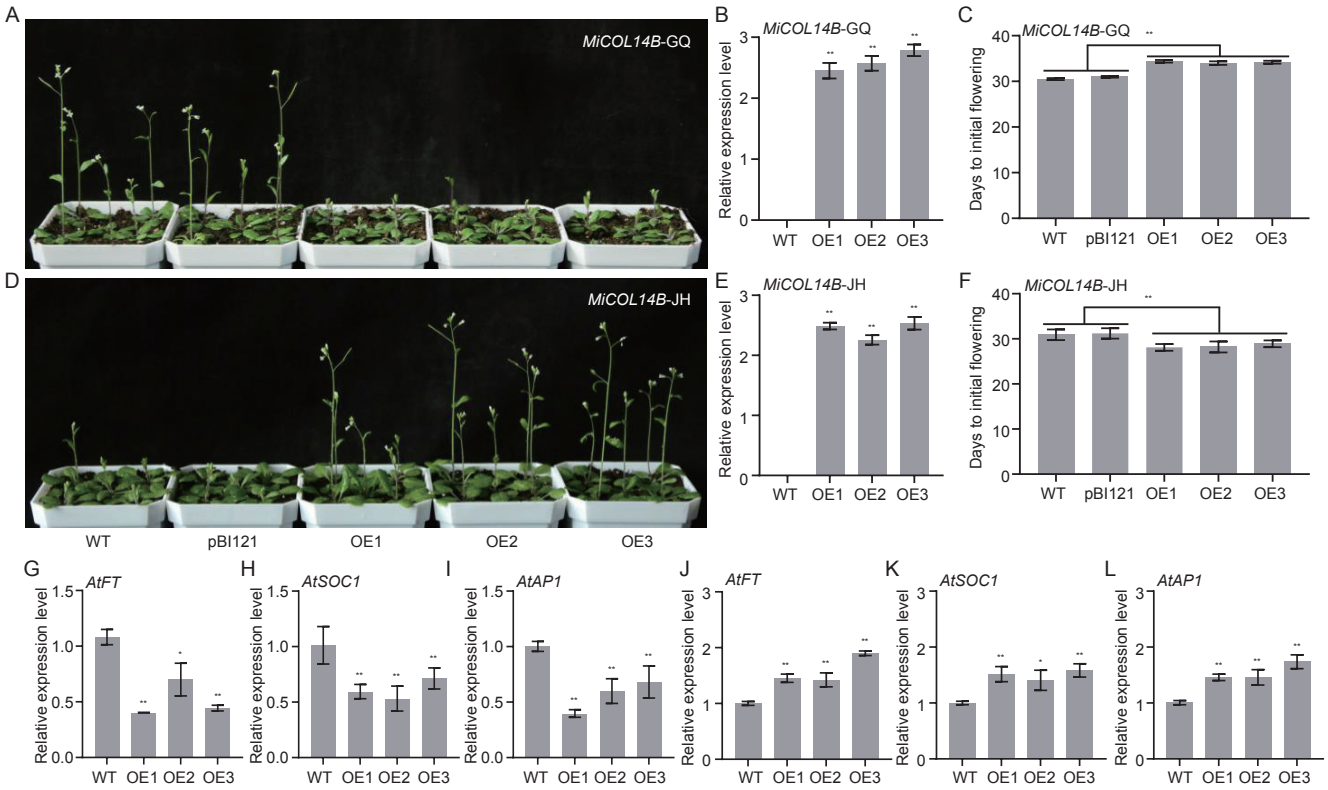

Fig. 3 Analysis of flowering phenotypes and endogenous flowering-related gene expression in *Arabidopsis thaliana* transgenic lines overexpressing *MiCOL14B*-GQ or *MiCOL14B*-JH under LD conditions. A, *MiCOL14B*-GQ overexpression delays flowering in *A. thaliana* under LD conditions. B, relative expression levels of *MiCOL14B*-GQ in the transgenic lines and WT plants. C, days to flowering for the *MiCOL14B*-GQ transgenic lines, WT, and pBI121 controls under LD conditions. D, *MiCOL14B*-JH overexpression promotes flowering in *A. thaliana* under LD conditions. E, relative expression levels of *MiCOL14B*-JH in transgenic lines and WT plants. F, days to flowering for the *MiCOL14B*-JH transgenic lines, WT, and pBI121 controls under LD conditions. G–I, expression profiles of flowering-promoting genes (*AtFT*, *AtSOC1*, *AtAP1*) in the *MiCOL14B*-GQ transgenic and WT lines. J–L, expression profiles of flowering-promoting genes (*AtFT*, *AtSOC1*, *AtAP1*) in the *MiCOL14B*-JH transgenic and WT lines. Data are presented as the mean±standard error (SE) (*n*=3). *, $P<0.05$; **, $P<0.01$ (two-tailed Student's *t*-test).

Temporal expression analysis revealed that both *MiCOL14B*-GQ and *MiCOL14B*-JH were expressed throughout all growth stages of mango, with significantly higher expression levels during key reproductive stages such as flower differentiation, inflorescence elongation, and flowering (Fig. 2-C and D). These results suggest that these two genes may be involved in regulating flower development. Furthermore, the expression patterns of *MiCOL14B*-GQ and *MiCOL14B*-JH under abiotic stress were investigated by treating mango plants with salt and simulated drought. Under salt stress, *MiCOL14B*-GQ expression peaked at approximately 24 h after treatment and subsequently decreased (Fig. 2-E), whereas *MiCOL14B*-JH expression peaked at 12 h after treatment (Fig. 2-F). Under simulated drought stress, both genes presented similar trends, with expression peaking at 36 h after treatment (Fig. 2-G and H).

3.3. Heterologous expression of the *MiCOL14B*-GQ and *MiCOL14B*-JH genes in *A. thaliana* alters their flowering time

To investigate the roles of *MiCOL14B*-GQ and *MiCOL14B*-JH in flowering regulation, we performed sowing experiments using homozygous transgenic *A. thaliana* lines (T_3 generation) and WT plants under LD conditions. The flowering time (from sowing to first flower opening), number of rosette leaves at bolting were recorded as phenotypic indicators. The expression of *MiCOL14B*-GQ and *MiCOL14B*-JH was confirmed in the transgenic *A. thaliana* plants *via* qRT-PCR, but not in the WT or pBI121 control plants (Fig. 3-B and E). Under LD conditions, the *MiCOL14B*-GQ and *MiCOL14B*-JH overexpression lines exhibited opposite effects on flowering time in *A. thaliana*. Phenotypic analysis revealed that the *MiCOL14B*-GQ overexpression line flowered 2–3 d later than the WT and pBI121 lines (Fig. 3-A and C), whereas the *MiCOL14B*-JH line flowered 2–3 d earlier (Fig. 3-D and F). Consistent with the observed phenotypic alterations, qRT-PCR analysis revealed that the expression levels of the flowering-promoting genes *AtFT*, *AtSOC1*, and *AtAP1* were significantly lower in the *MiCOL14B*-GQ transgenic line than in the WT control (Fig. 3-G–I). Conversely, these genes were significantly upregulated in the *MiCOL14B*-JH line (Fig. 3-J–L), indicating that *MiCOL14B*-JH accelerates flowering by activating the floral integrator pathway.

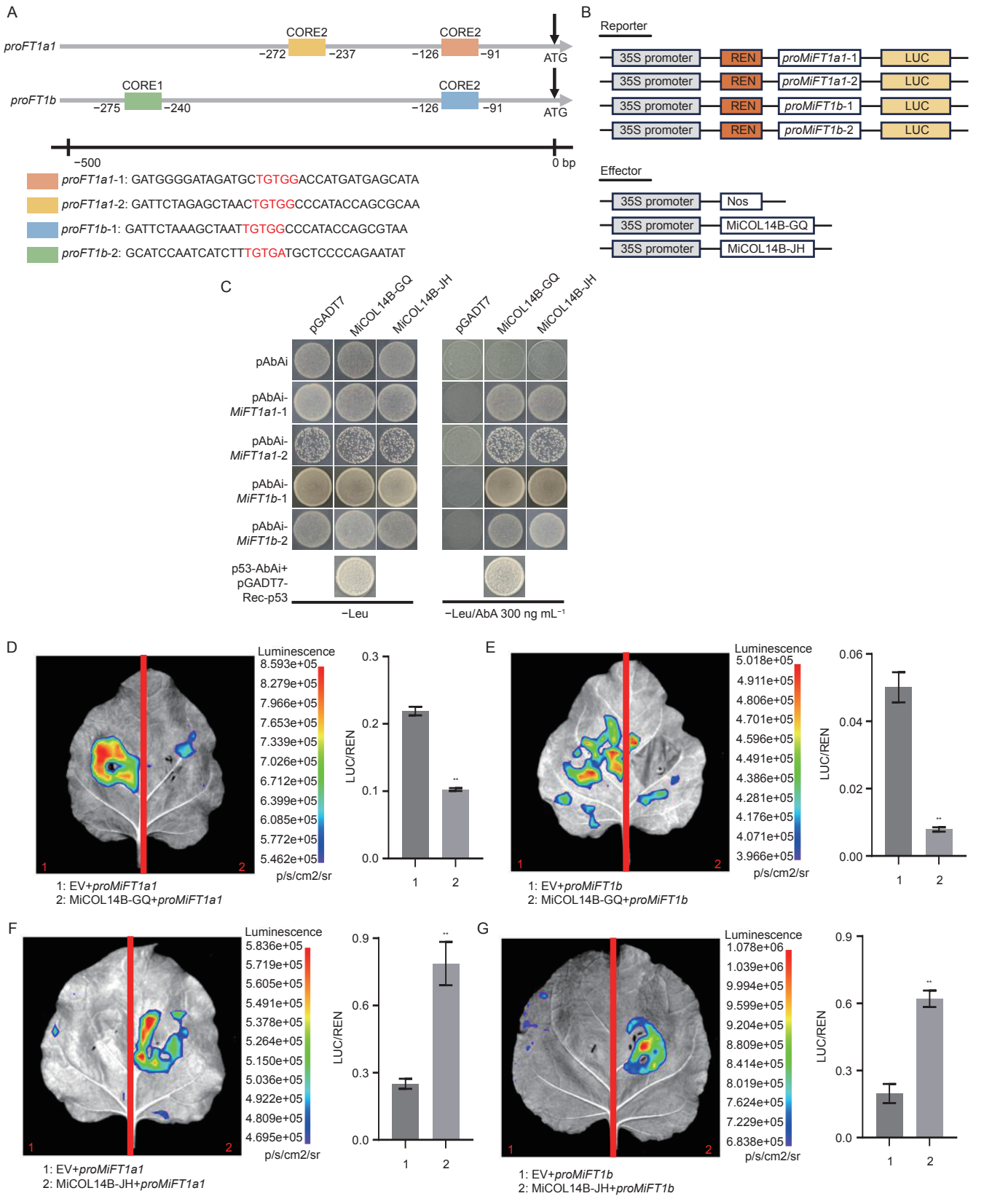

Fig. 4 Y1H and dual luciferase reporter assays. A, schematic diagram of the promoter regions of *MiFT1a1* and *MiFT1b*, highlighting the positions of CORE1 and CORE2 elements with specific base coordinate ranges. B, construction of the reporter and effector genes used in the Y1H experiments. C, Y1H assays confirmed that MiCOL14B-GQ and MiCOL14B-JH can bind to the CORE1 and CORE2 elements in the *MiFT* promoter, with p53-AbAi+pGADT7-Rec-p53 used as a positive control. D–G, quantitative analysis of the interaction between MiCOL14B-GQ and MiCOL14B-JH with the *MiFT1a1* and *MiFT1b* promoters. Numbers 1 and 2 indicate distinct experimental groups, respectively, while EV stands for empty vector. Data are presented as the mean±standard error (SE) (n=3). *, P<0.05; **, P<0.01 (two-tailed Student's t-test).

3.4. MiCOL14B-GQ and MiCOL14B-JH directly bind to the promoters of *MiFT1a1* and *MiFT1b* and regulate their activities

According to previous reports, CO/COL reportedly bind to the CORE1 (TGTGA), CORE2 (TGTGG), P1 (CCACA), and P2 (TGTGG) regions within the *FT* promoter, thereby increasing *FT* transcription (Lv *et al.* 2021). To verify whether mango CO/COL proteins bind to the promoters of *MiFT1a1* and *MiFT1b*, we analysed their promoter regions. Two conserved CORE2 motifs were identified in the *MiFT1a1* promoter and designated *MiFT1a1*-1 and *MiFT1a1*-2. In contrast, the *MiFT1b* promoter contained one CORE1 motif and one CORE2 motif, which were named *MiFT1b*-1 and *MiFT1b*-2, respectively. Based on these CORE1 and CORE2 sequences, we amplified approximately 35-bp promoter fragments, each encompassing the target binding motif flanked by ~15 bp of upstream and downstream sequence. These fragments were then cloned into the pAbAi vector to generate bait constructs for Y1H assays (Fig. 4-A).

Y1H assays demonstrated that both MiCOL14B-GQ and MiCOL14B-JH specifically bind to the two identified CORE2 motifs (*MiFT1a1*-1 and *MiFT1a1*-2) in the *MiFT1a1* promoter, as well as to the CORE1 (*MiFT1b*-2) and CORE2 (*MiFT1b*-1) motifs in the *MiFT1b* promoter (Fig. 4-C). To validate these interactions and assess their functional impact, we performed dual-luciferase reporter assays (Fig. 4-B). The results revealed opposing regulatory roles for the two proteins. MiCOL14B-GQ acted as a repressor, significantly suppressing the activity of both the *MiFT1a1* and *MiFT1b* promoters. The LUC/REN ratio was reduced to approximately 50% of the control level for the *MiFT1a1* promoter (Fig. 4-D) and to about 14% for the *MiFT1b* promoter (Fig. 4-E). In contrast, MiCOL14B-JH functioned as a strong activator, enhancing the LUC/REN ratio by approximately 3.1-fold for the *MiFT1a1* promoter and 3.3-fold for the *MiFT1b* promoter compared to the control (Fig. 4-F and G).

3.5. Overexpression of *MiCOL14B*-GQ and *MiCOL14B*-JH enhances *A. thaliana* tolerance to salt and drought stress

Under salt stress, both transgenic lines developed significantly longer roots than the WT, demonstrating enhanced salt tolerance (Figs. 5-A and C; 6-A and C). The survival rates of the *MiCOL14B*-GQ and *MiCOL14B*-JH overexpression lines following salt treatment were also markedly higher than those of the WT (Figs. 5-B and 6-B). Specifically, the survival rates for *MiCOL14B*-GQ lines were 87.5%, 90.5%, and 82.75% per pot, compared to only 20% for the WT (Fig. 5-E). Similarly, the survival rates for *MiCOL14B*-JH lines reached 85%, 82.5%, and 90%, whereas the WT survival rate was merely 30% (Fig. 6-E). Consistent with these phenotypic results, qRT-PCR analysis revealed significant upregulation of the ion homeostasis genes *AtSOS1* and *AtNHX1* and the stress-responsive transcription factor *AtDREB2A* in the transgenic lines. These results suggest that both *MiCOL14B*-GQ and *MiCOL14B*-JH enhance salt tolerance by promoting ion homeostasis and activating stress-responsive signaling pathways (Figs. 5-H–J; 6-H–J).

Under simulated drought stress, the root lengths of both *MiCOL14B*-GQ and *MiCOL14B*-JH overexpression lines were significantly longer than those of the WT (Figs. 5-A and D; 6-A and D). To further evaluate drought tolerance, seedlings were subjected to 26 d of water deprivation followed by 3 d of re-watering. The overexpression lines of both *MiCOL14B*-GQ and *MiCOL14B*-JH exhibited significantly higher survival rates compared to the WT (Figs. 5-B and 6-B). Specifically, the survival rates for the three independent *MiCOL14B*-GQ lines were 67.5%, 75.45%, and 82.75%, respectively, in stark contrast to the mere 12.5% survival rate of the WT (Fig. 5-E). Similarly, the *MiCOL14B*-JH lines showed survival rates of 78.8%, 80.7%, and 83.5%, while the survival rate of the WT was 0% (Fig. 6-E). The increased expression of the dehydration-protective genes *AtCOR15A* and *AtRD29A* and the stress marker *AtKIN1* further indicated the activation of osmotic regulation and stress adaptation pathways (Figs. 5-K–M; 6-K–M). In summary, the overexpression of *MiCOL14B*-GQ and *MiCOL14B*-JH improved *A. thaliana* tolerance to salt and drought stresses. This enhanced adaptability is likely mediated by the coordinated upregulation of salt-responsive genes and drought-responsive genes, highlighting the dual roles of these two genes in mediating stress signalling cascades and cellular protective mechanisms.

3.6. Assessment of physiological stress indicators

Staining with NBT, Evans blue, and DAB revealed that *MiCOL14B*-GQ or *MiCOL14B*-JH overexpressing lines of *A. thaliana* accumulated significantly less $O_2^{\cdot-}$ and H_2O_2 than WT, and maintained greater membrane integrity (Figs. 5-G and 6-G). These results indicate that the transgenic lines possess greater antioxidant capacity and more stable membrane systems. Consistent with the staining results, physiological assays showed that the transgenic lines had significantly higher SOD activity and proline content, as well as significantly lower MDA and H_2O_2 levels, compared to the WT control (Figs. 5-F and 6-F). Collectively, these data confirm that both *MiCOL14B*-GQ and *MiCOL14B*-JH alleviate oxidative damage *via* two coordinated mechanisms: increasing antioxidant enzyme activity and improving the osmotic adjustment capacity. These findings strongly illustrate that *MiCOL14B*-GQ and *MiCOL14B*-JH increase stress tolerance by systematically regulating oxidative stress response cascades.

3.7. *MiCOL14B*-GQ/JH increases salt and drought stress tolerance in hairy roots of transgenic mango plants

Transgenic mango hairy roots were successfully obtained by transforming mango hypocotyls with *A. rhizogenes* (Fig. 7-A). Total RNA was extracted from the newly formed roots and reverse-transcribed into cDNA for PCR analysis. The PCR products showing a single band of the expected size were sequenced to confirm the successful integration of the target genes (Appendix B). Furthermore, qRT-PCR analysis demonstrated that both *MiCOL14B*-GQ and *MiCOL14B*-JH were highly expressed in their respective transgenic root lines compared to the controls (Appendix B), confirming successful

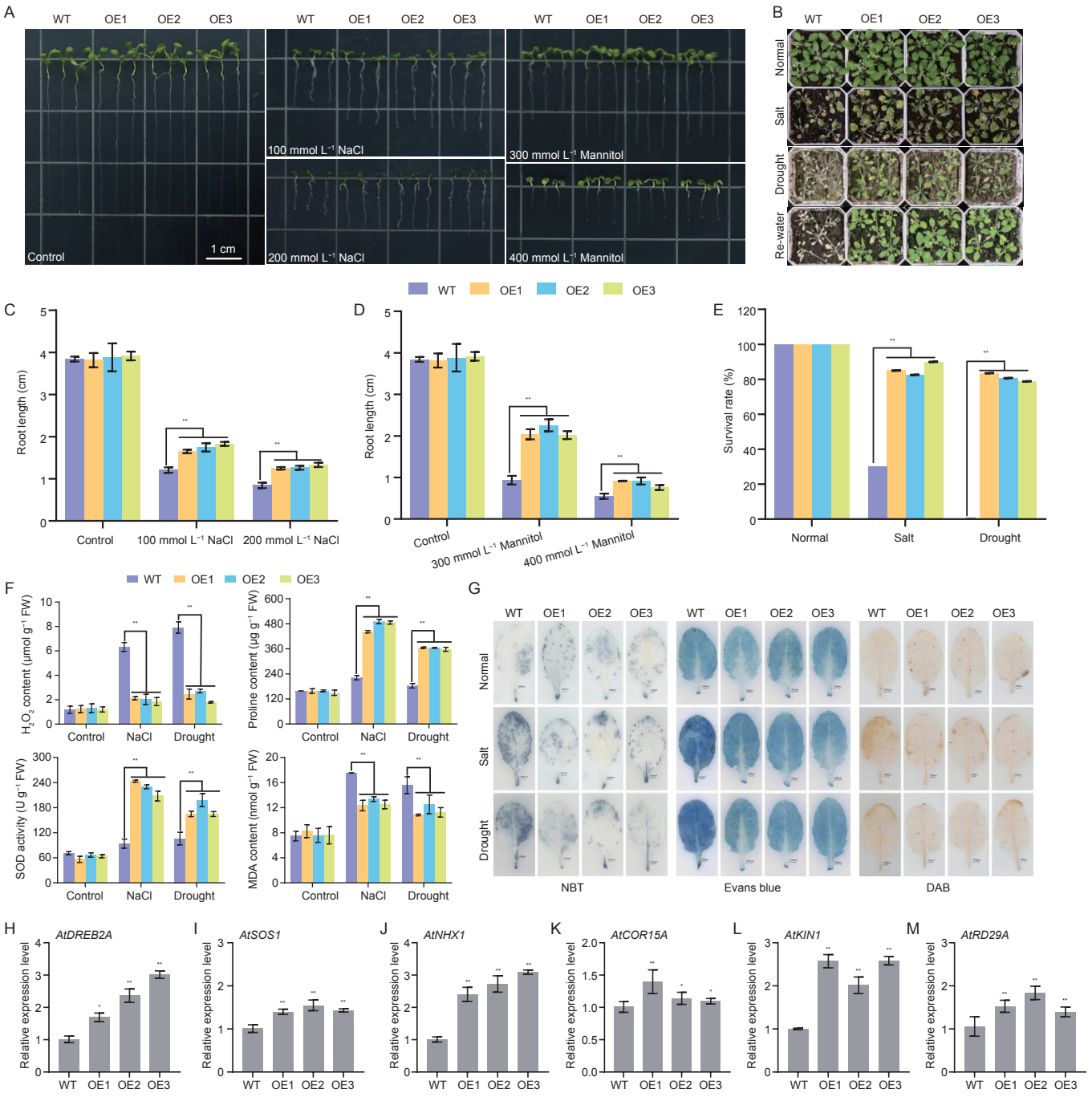

Fig. 5 Analysis of stress tolerance in *MiCOL14B*-GQ transgenic lines under salt and drought stresses. A, root length phenotypes of WT and transgenic plants under stress conditions, with scale bars indicating 1.0 cm. B, morphological observations under the control, salt, and drought treatments. C and D, measurements of root elongation under normal, salt and drought stress conditions. E, survival rate comparison between WT and *MiCOL14B*-GQ transgenic plants after 7 d of stress treatment. F, contents of H_2O_2, Pro and MDA, and enzymatic activity of SOD in WT and transgenic lines under non-stressed and stressed conditions. G, histochemical staining results for reactive oxygen species (ROS) *via* DAB (H_2O_2), Evans blue (cell membrane integrity), and NBT (superoxide radicals) in WT and transgenic leaves. H–M, relative expression profiles of stress-responsive genes (*AtDREB2A*, *AtSOS1*, *AtNHX1*, *AtCOR15A*, *AtKIN1* and *AtRD29A*) in *MiCOL14B*-GQ transgenic and WT plants following salt and drought treatment. Data are presented as the mean±standard error (SE) (n=3). *, P<0.05; **, P<0.01 (two-tailed Student's t-test).

transgene transcription. After molecular verification, we ultimately obtained seven independent *MiCOL14B*-GQ and eight independent *MiCOL14B*-JH transgenic hairy root lines. For the subsequent salt and simulated drought stress assays, two independent transgenic lines with consistent growth were selected from each construct for phenotypic evaluation.

The results demonstrated that under both salt and drought stress conditions, the stress tolerance of transgenic hairy roots overexpressing *MiCOL14B*-GQ or *MiCOL14B*-JH was significantly enhanced compared to the empty vector control. Physiologically, the transgenic hairy roots exhibited significantly higher proline content and SOD activity (Fig. 7-B and D), along

with significantly lower levels of MDA and H_2O_2 following stress treatments (Fig. 7-C and E). These findings indicate that *MiCOL14B*-GQ and *MiCOL14B*-JH activate defense responses in transgenic hairy roots, enabling them to mitigate salt and drought stress damage through coordinated physiological adjustments and thereby improving stress tolerance.

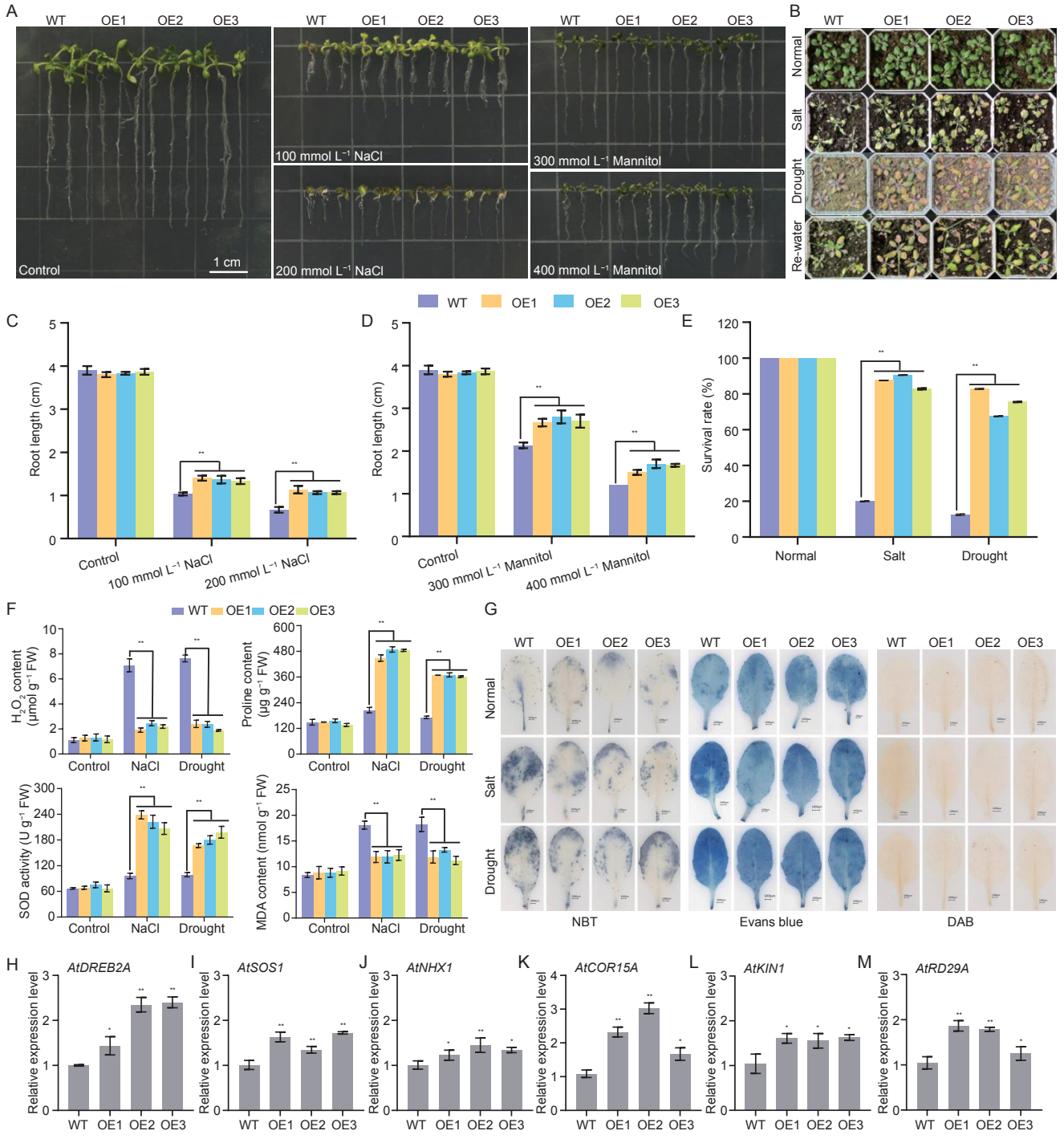

Fig. 6 Analysis of stress tolerance in *MiCOL14B*-JH transgenic lines under salt and drought stresses. A, root length phenotypes of WT and transgenic plants under stress conditions, with scale bars indicating 1.0 cm. B, morphological observations under control, salt, and drought treatments. C and D, measurements of root elongation under normal, salt and drought stress conditions. E, survival rate comparison between WT and *MiCOL14B*-JH transgenic plants after 7 d of stress treatment. F, contents of H_2O_2, Pro and MDA, and enzymatic activity of SOD in WT and transgenic lines under non-stressed and stressed conditions. G, histochemical staining results for reactive oxygen species (ROS) *via* DAB (H_2O_2), Evans blue (cell membrane integrity), and NBT (superoxide radicals) in WT and transgenic leaves. H–M, relative expression profiles of stress-responsive genes (*AtDREB2A*, *AtSOS1*, *AtNHX1*, *AtCOR15A*, *AtKIN1* and *AtRD29A*) in *MiCOL14B*-JH transgenic and WT plants following salt and drought treatment. Data are presented as the mean±standard error (SE) (n=3). *, P<0.05; **, P<0.01 (two-tailed Student's t-test).

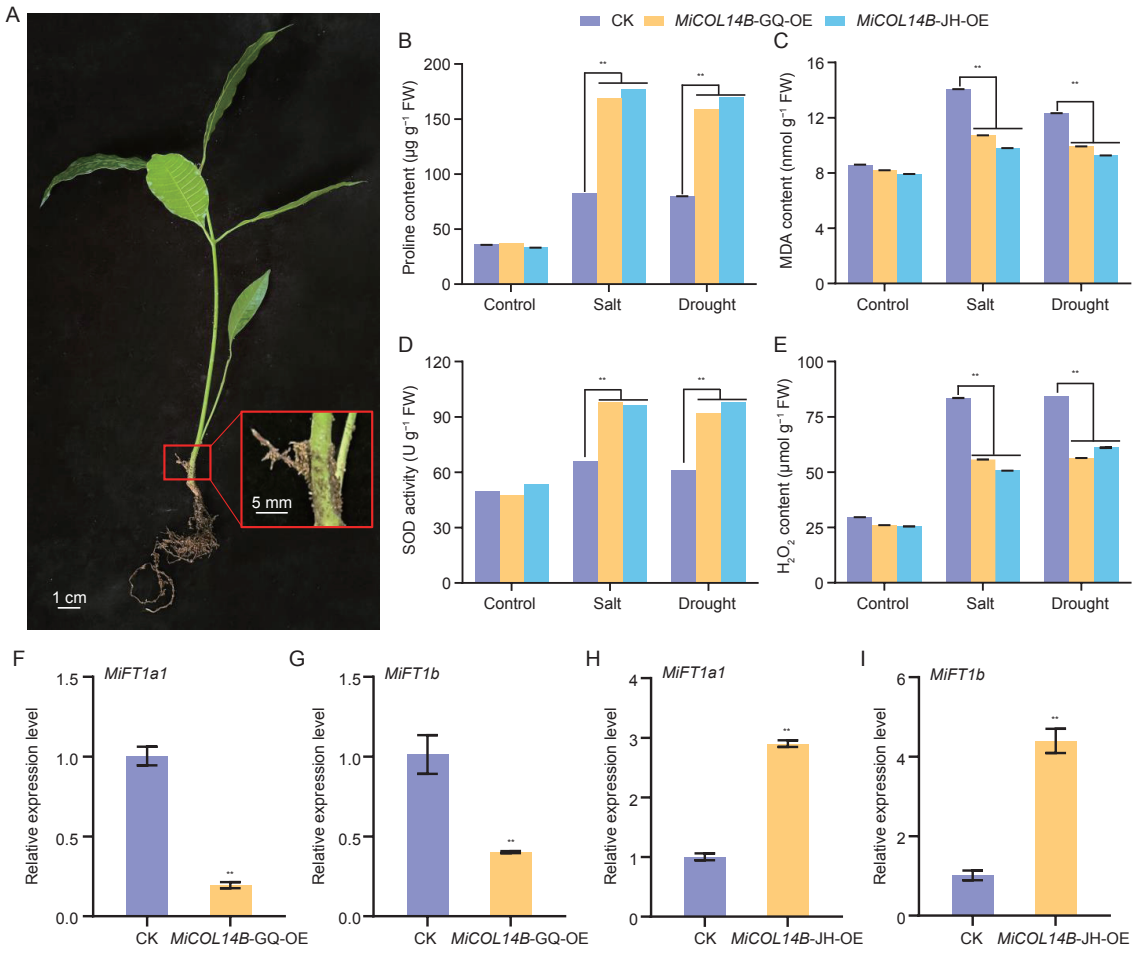

Fig. 7 Phenotypic and physiological traits of transgenic hairy roots under stress conditions and analysis of endogenous flowering genes. A, one month old transgenic hairy roots. B–E, contents of MDA, Pro, and H_2O_2, as well as the enzymatic activities of SOD. F and G, effects of *MiCOL14B*-GQ overexpression in hairy roots on *MiFT1a1* and *MiFT1b* expression levels. H and I, effects of *MiCOL14B*-JH overexpression in hairy roots on *MiFT1a1* and *MiFT1b* expression levels. Data are presented as the mean±standard error (SE) (*n*=3). *, *P*<0.05; **, *P*<0.01 (two-tailed Student's *t*-test).

3.8. *MiCOL14B*-GQ/JH overexpression modulated *MiFT1a1* and *MiFT1b* expression

qRT-PCR was performed to investigate the regulatory roles of *MiCOL14B*-GQ and *MiCOL14B*-JH in the expression of flowering-associated genes. Specifically, three independent transgenic hairy root lines were selected per gene to ensure reliability. The results showed overexpression of *MiCOL14B*-GQ significantly downregulated the transcript levels of the flowering integrator genes *MiFT1a1* and *MiFT1b* (Fig. 7-F and G). In contrast, overexpression of *MiCOL14B*-JH markedly upregulated the expression of the same genes (Fig. 7-H and I). These results confirm the distinct regulatory functions of *MiCOL14B*-GQ and *MiCOL14B*-JH in mango floral regulation, highlighting their importance in the transition from vegetative to reproductive growth.

3.9. Interaction verification between MiCOL14B-GQ and MiCOL14B-JH proteins and MiWRKYs proteins and abiotic stress-related proteins

To assess the suitability of MiCOL14B-GQ and MiCOL14B-JH for Y2H screening, we first tested their potential transcriptional self-activation activity in Y2HGold yeast cells. On selective media (SD/–Trp/X-α-gal/AbA), yeast cells harboring BD-MiCOL14B-GQ or BD-MiCOL14B-JH developed distinct blue coloration and demonstrated robust growth, confirming that both proteins possess intrinsic autoactivation activity. In contrast, cells expressing truncated variants lacking the middle region (BD-MiCOL14B-GQ-ΔMR and BD-MiCOL14B-JH-ΔMR) neither grew nor turned blue under the same conditions (Fig. 8-A). These results demonstrate that the transcriptional autoactivation of both MiCOL14B-GQ and MiCOL14B-JH is strictly dependent on their intact middle domain (MR). Deletion of the MR completely abrogated their self-activation capacity, thus enabling the use of BD-MiCOL14B-GQ-ΔMR and BD-MiCOL14B-JH-ΔMR as valid bait constructs for subsequent Y2H interaction screening.

Y2H assays were performed to identify the interaction partners of MiCOL14B-GQ and MiCOL14B-JH. Both proteins interacted with the WRKY transcription factors MiWRKY12a, MiWRKY12A, MiWRKY12B, MiWRKY13A, and MiWRKY13B. Furthermore, MiCOL14B-GQ specifically interacted with

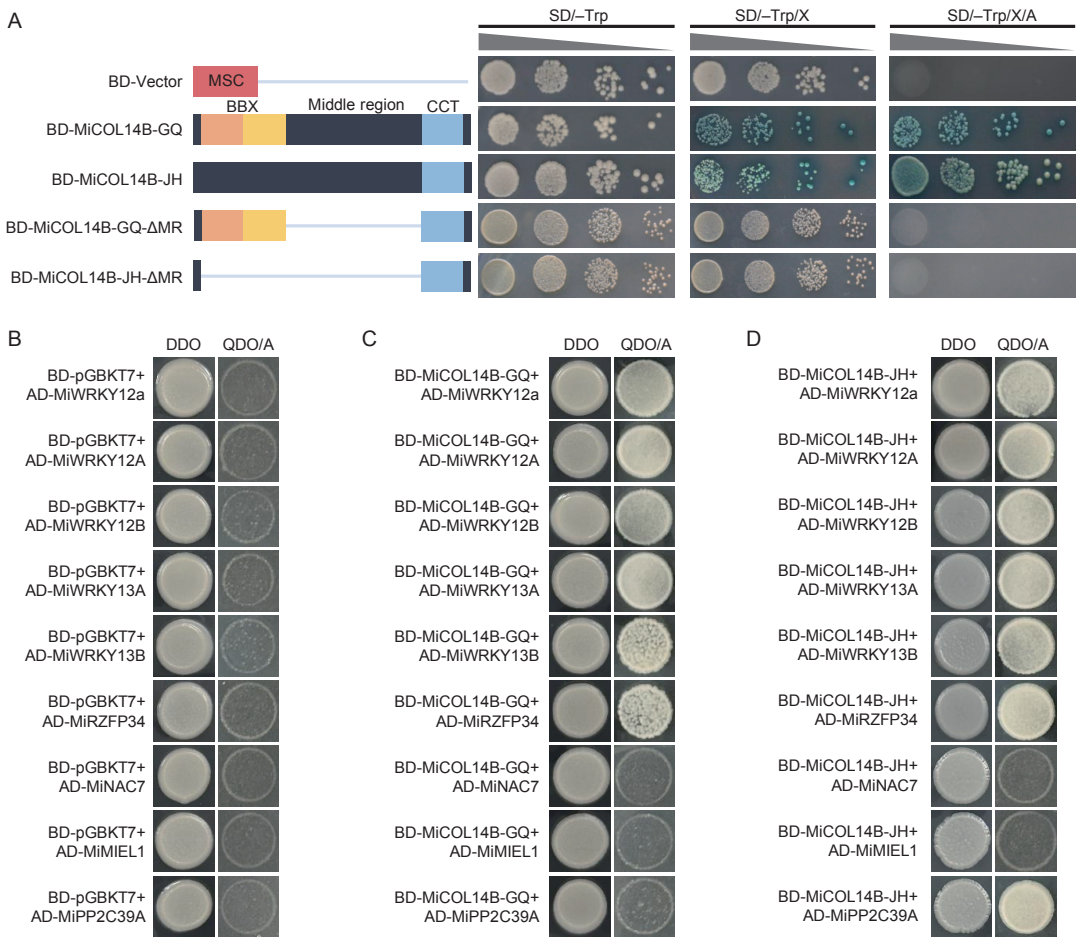

Fig. 8 Y2H validation of MiCOL14B-GQ and MiCOL14B-JH with candidate proteins. A, autoactivation validation of MiCOL14B-GQ and MiCOL14B-JH. B, autoactivation validation of candidate proteins. C and D, Y2H results of MiCOL14B-GQ and MiCOL14B-JH.

the zinc finger protein MiRZFP34, whereas MiCOL14B-JH interacted with both MiRZFP34 and the protein phosphatase MiPP2C39A (Fig. 8-C and D). Prior to Y2H interaction detection, all candidate proteins were confirmed to exhibit no self-activation activity, ensuring the reliability of the experimental results (Fig. 8-B), which effectively ruled out false-positive interactions and guaranteed the reliability of the Y2H results.

3.10. Subcellular localization and BiFC analysis

To validate the predicted nuclear localization of MiCOL14B-GQ and MiCOL14B-JH, we performed transient expression assays in inner epidermal cells of onion bulbs. Confocal microscopy using a Leica TCS-SP8 system showed that the green fluorescent protein (GFP) control (empty vector) was diffusely distributed in the cytoplasm and nucleus, whereas the MiCOL14B-GQ-GFP and MiCOL14B-JH-GFP fusion proteins displayed exclusive nuclear localization (Fig. 9-A). This nuclear confinement is consistent with Plant-mPLoc predictions and supports their putative functions as transcriptional regulators.

BiFC assays were performed to verify the physical interactions between MiCOL14B-GQ or MiCOL14B-JH and their candidate partners. Recombinant plasmids harboring MiCOL14B-GQ-NE or MiCOL14B-JH-NE were co-expressed with plasmids carrying MiWRKYs-CE in the inner epidermal cells of onion bulbs. Reconstituted yellow fluorescent protein (YFP) signals were specifically detected in the nucleus, and DAPI counterstaining further confirmed that the interaction-derived fluorescence signals were localized to the nucleus. (Fig. 9-C and D). For stress-related interacting partners, distinct nuclear fluorescence was detected in three combinations: MiCOL14B-GQ-NE+MiRZFP34-CE, MiCOL14B-JH-NE+MiRZFP34-CE, and MiCOL14B-JH-NE+MiPP2C39A-CE (Fig. 9-C and D). No fluorescence was detected in the negative controls co-expressing MiCOL14B-GQ-NE or MiCOL14B-JH-NE with the empty pSPYCE vector (Fig. 9-B).

4. Discussion

4.1. The *COL* gene family has diverse functions and mechanisms for regulating plant flowering

In *A. thaliana*, *CO* acts as the central regulator of the photoperiod flowering pathway (Shim *et al.* 2017). In rice, the overexpression of *OsCOL5* results in delays flowering, as well as increases plant height, number of main panicles, total grain number per plant, and plant yield under both LD and SD conditions (Wen *et al.* 2024). In mungbean (*Vigna radiata*), overexpression of *VrCOL2* accelerates flowering in transgenic *A. thaliana* under SD conditions by regulating

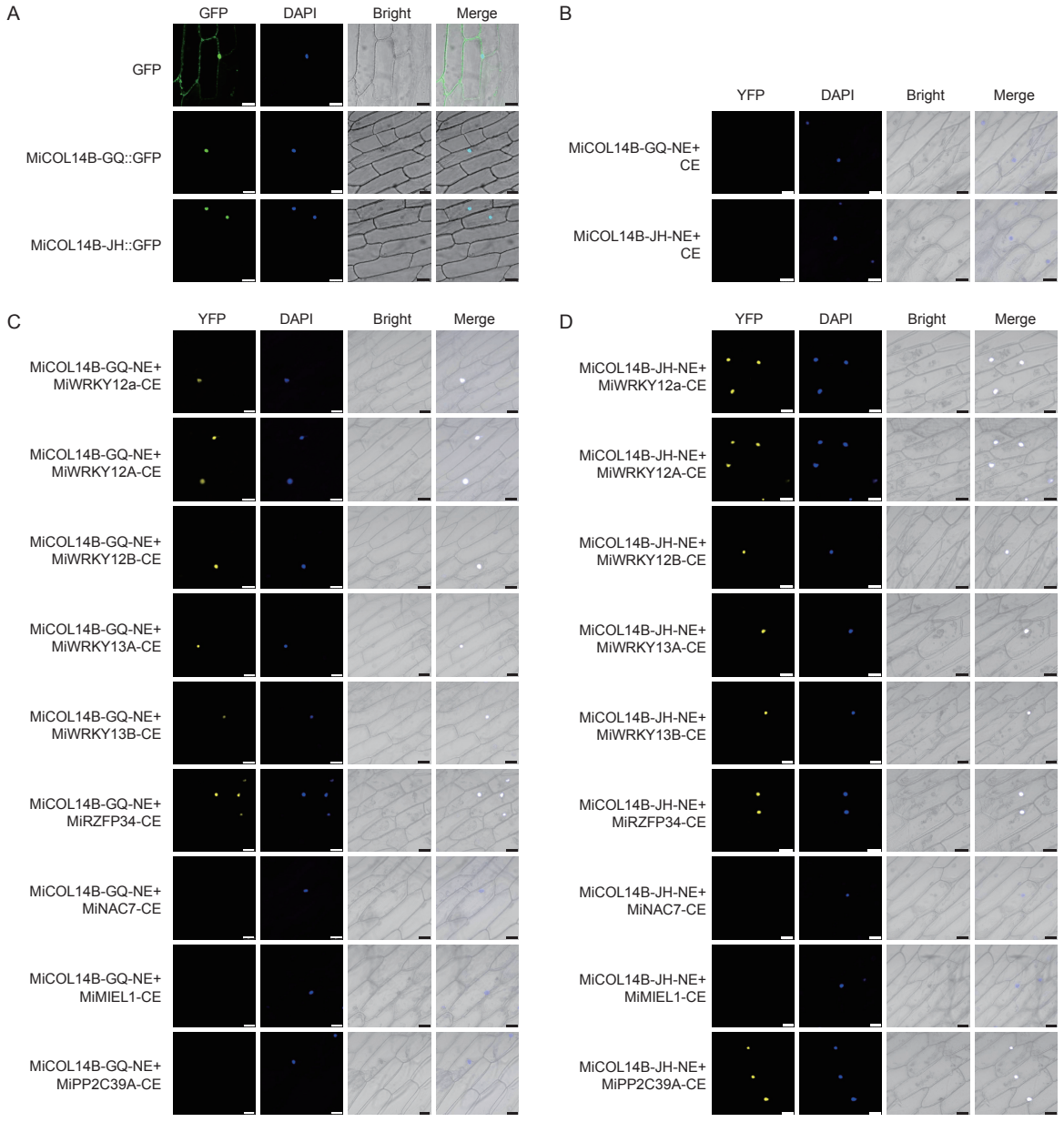

Fig. 9 Subcellular localization and BiFC assays of the MiCOL14B-GQ and MiCOL14B-JH proteins. A, subcellular locations of MiCOL14B-GQ and MiCOL14B-JH. B, negative controls for BiFC assays using MiCOL14B-GQ/JH-NE and empty CE vectors co-expressed without target proteins. C and D, BiFC assay results for MiCOL14B-GQ and MiCOL14B-JH. Bars=75 μm.

the expression of the flowering time gene *AtFT* (Liu *et al.* 2021). In *Liriodendron chinense*, the overexpression of *LcCO* significantly increases flowering time and reduces rosette leaf number in transgenic *A. thaliana* under LD conditions (Cui *et al.* 2023). In common bean, *COL2* represses *FT* expression under LD conditions, thereby delaying flowering (González *et al.* 2021). In Longan, *DlCOL4* negatively regulates flowering when it is heterologously expressed in transgenic *A. thaliana* (Gou *et al.* 2025). Collectively, these findings illustrate that the *CO*/*COL* gene family exhibits distinct functional divergence in mediating flowering regulation across plant species. In this study, the *MiCOL14B*-GQ variant contains two B-box domains that act as flowering repressors, whereas *MiCOL14B*-JH, a variant lacking B-box domains, functions as a flowering promoter. In our previous work, we identified two structural variants of *MiCOL14A* in diverse mango cultivars: *MiCOL14A*-GQ and *MiCOL14A*-JH. Both variants harbor two B-box domains and consistently delay flowering when overexpressed in transgenic *A. thaliana* (Chen *et al.* 2023). Comparative analysis of the structure-function relationships between *MiCOL14A* and *MiCOL14B* variants highlights that the B-box domain plays a pivotal role in mango flowering regulation: the presence of an intact B-box domain likely suppresses flowering *via* specific molecular mechanisms, whereas the loss of these domains eliminates the repressive effect and induces flowering. Notably, B-box motifs, especially their conserved residues, are well known to mediate protein-protein interactions and modulate transcriptional regulation in various plant systems (Gangappa *et al.* 2013).

4.2. The regulatory network formed by *MiCOL14B*-GQ/JH and *MiFT*s influences plant flowering by modulating the *CO-FT* pathway

The expression of the *CO* gene in response to photoperiod is coordinated by a complex network of transcription factors and signaling cascades. In *A. thaliana*, *CO* is established as the key mediator of photoperiodic flowering (Shim *et al.* 2017). The *CO-FT* pathway is the core pathway through which plants respond to photoperiodic variations and regulate flowering time. As the central integrator of photoperiod signals, *CO* promotes the expression of the *FT* gene, whose encoded florigen translocates from the leaves to the SAM (Wigge *et al.* 2005; Corbesier *et al.* 2007), where it forms a complex with the BASIC LEUCINE ZIPPER (bZIP) transcription factor FD. This complex then initiates the expression of downstream floral identity genes, including *SOC1* and *AP1* (Putterill *et al.* 1995; Onouchi *et al.* 2000; Corbesier *et al.* 2007; Lee and Lee 2010). The activation of this pathway is tightly controlled by light. Photoreceptors such as phytochromes and cryptochromes perceive red and blue light, leading to both transcriptional regulation of the *CO* gene and post-translational modulation of CO protein stability. These regulatory events collectively activate the expression of the florigen-encoding gene *FT* to promote floral transition. (Böhlenius *et al.* 2006; Wang *et al.* 2024). Tiwari *et al.* (2010) were the first to biochemically confirm the direct binding of CO to the *FT* promoter. Further research has demonstrated that this direct binding directly activates transcription, thereby triggering floral transition through the photoperiodic flowering pathway. In rose (*Rosa chinensis*), RcCOL4 and RcCO interact with each other, and promote RcCO binding to the CORE motif in the *RcFT* promoter, thus inducing *RcFT* expression. Meanwhile, silencing either *RcCO* or *RcCOL4* delays flowering (Lu *et al.* 2020). Under SD conditions, the *CO-FT* pathway can promote the flowering of 'Jiaobai' (*Zizania latifolia*). Specifically, ZlCOL1 binds to the promoter of the *FT* gene *Gall Swelling Date 1* (*ZlGsd1*) and activates its transcription to promote flowering (Zhang *et al.* 2024).

In this study, we identified two CO-binding sites (CORE1 and CORE2) in the promoters of *MiFT*s. Y1H and dual-luciferase reporter assays demonstrated that MiCOL14B-GQ bound to these sites and significantly suppressed *MiFT*s promoter activity. In contrast, MiCOL14B-JH enhanced this activity, suggesting their opposing roles in *FT* regulation. Consistent with this, analysis in transgenic hairy roots confirmed that *MiCOL14B*-GQ acts as a repressor of *MiFT1a1* and *MiFT1b*, while *MiCOL14B*-JH functions as an activator of these two genes. Integrating these results with the *FT* expression data from *A. thaliana*, these findings suggest that *MiCOL14B*-GQ may delay flowering by inhibiting the floral integrator pathway, whereas *MiCOL14B*-JH promotes early flowering by activating this pathway. This model is further supported by prior evidence establishing *MiFT1a1* and *MiFT1b* as flowering promoters in plants (Li *et al.* 2024).

4.3. *COL* genes exhibit multifunctional regulation in salt and drought stress responses

Plants regulate their flowering time to adapt to environmental changes, ensuring reproduction under the most favourable conditions, which is crucial for their survival and propagation (Niu *et al.* 2024). Recent studies highlight the critical role of the *COL* gene family in abiotic stress regulation. In *A. thaliana*, *CO* negatively regulates plant tolerance to salt stress (Du *et al.* 2023). In soybean, *GmCOL1a* is induced under salt and drought stress and enhances adaptation by reducing the Na^+/K^+ ratio to maintain ion homeostasis (Xu *et al.* 2023). Similarly, in *Andrographis paniculata*, salt stress upregulates *ApCOL8*, and its heterologous expression in yeast improves salt tolerance (Zhao *et al.* 2025). In this study, *MiCOL14B*-GQ and *MiCOL14B*-JH enhanced plant stress resistance by regulating the oxidative stress pathway. Under salt and drought stress, transgenic hairy roots overexpressing *MiCOL14B*-GQ or *MiCOL14B*-JH showed increased SOD activity and proline content, reduced H_2O_2 accumulation, and decreased MDA levels, thereby maintaining cell membrane integrity. Similarly, in transgenic *A. thaliana* plants, *MiCOL14B*-GQ and *MiCOL14B*-JH effectively alleviated oxidative stress by modulating the antioxidant defense system and osmotic balance, thereby improving plant tolerance to salt and drought stress. Moreover, these transgenic plants increased stress tolerance by increasing the expression of stress-related genes, enhancing ion exclusion capacity, and increasing stress signal transduction. These results are consistent with previous studies from our research group, indicating that *MiCOL1* (Guo *et al.* 2022), *MiCOL2* (Liang *et al.* 2023), and *MiCOL16* (Liu *et al.* 2022a) increase the survival rate and stress tolerance of transgenic lines under salt and drought conditions. Notably, transgenic *A. thaliana* plants expressing *MiCOL14A*-GQ presented increased sensitivity to salt stress, whereas those expressing the CCT domain-deficient variant *MiCOL14A*-JH presented enhanced drought tolerance. These results indicate that the CCT domain is essential for mediating plant responses to abiotic stresses (Chen *et al.* 2023). Collectively, these results underscore the pivotal role of mango *COL* genes in abiotic stress tolerance and their potential as valuable genetic resources for improving crop resilience through breeding.

4.4. Interaction network between COL proteins and stress-responsive factors

Interactions between CO/COL proteins and other abiotic stress-related proteins can increase plant tolerance to abiotic stresses. MdCOL9 interacts with MdMIEL1 to increase drought tolerance in apple (Chen *et al.* 2022). *GmCOL1a* enhances salt and drought tolerance in transgenic soybean hairy roots by promoting the accumulation of the Delta (1)-pyrroline-5-carboxylate synthetase (GmP5CS) protein (Xu *et al.* 2023). Under LD conditions during salt stress, CO interacts with and antagonizes ABSCISIC ACID-RESPONSIVE ELEMENT BINDING FACTOR (ABF) transcription factors, reducing plant salt tolerance (Du *et al.* 2023). Y2H and BiFC assays confirmed that both MiCOL14B-GQ and MiCOL14B-JH physically interact with MiWRKYs and the stress-related proteins MiRZFP34 and MiPP2C39A. Specifically, MiCOL14B-GQ interacted with MiWRKYs transcription factors and MiRZFP34, whereas MiCOL14B-

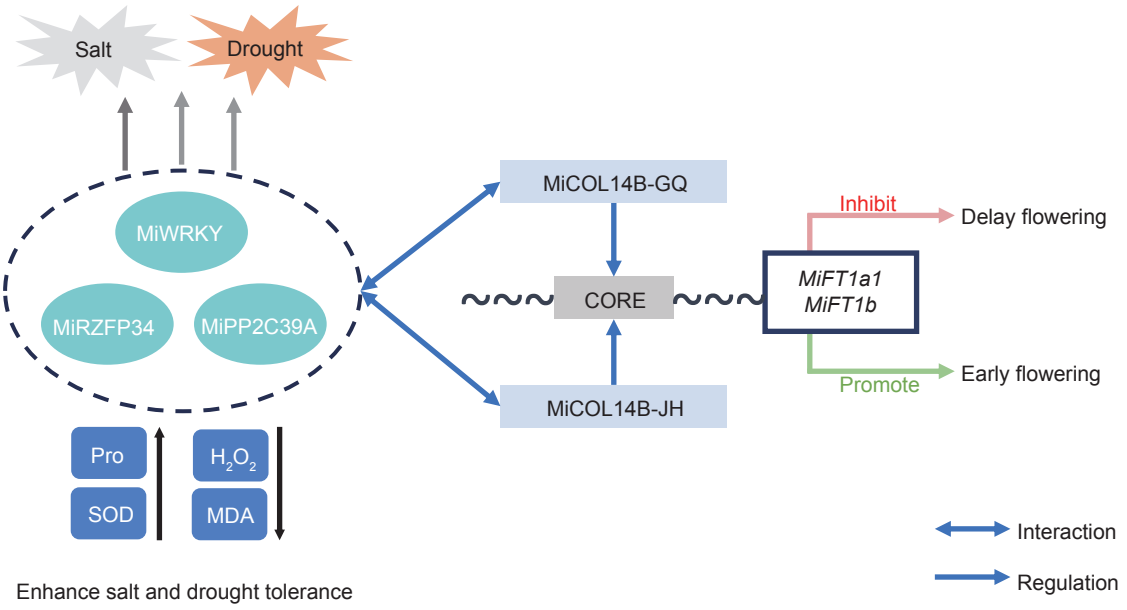

Fig. 10 Working model of the MiCOL14B-GQ and MiCOL14B-JH genes.

JH showed a broader range of interaction partners, including MiWRKYs, MiRZFP34, and MiPP2C39A. The observed divergence in interaction patterns between the two isoforms is likely attributed to differences in their structural domains. Our previous study identified two *MiCOL14A* structural variants, namely the CCT domain-deficient *MiCOL14A*-JH and the full-length *MiCOL14A*-GQ. Interaction assays demonstrated that MiCOL14A-JH binds MiZFP4 and MiMIEL1, whereas MiCOL14A-GQ lacks this binding capacity (Chen *et al.* 2023). The structural integrity of CO protein domains directly governs their binding specificity to DNA *cis*-elements and interaction partners, which in turn modulates their regulatory functions in flowering time control and stress adaptation. In previous studies, *MiRZFP34* confers tolerance to drought and cold (Lu *et al.* 2023). *PP2C* genes play a significant role in ABA signalling pathways (Ruan *et al.* 2024). Notably, our study is the first to identify protein–protein interactions between MiCOLs and MiWRKYs, suggesting that the two protein families may function synergistically. WRKY proteins are well documented regulators of plant stress responses. For example, heterologous overexpression of *ZmWRKY71* enhance drought tolerance in yeast and *A. thaliana* (Ma *et al.* 2025). The overexpression of *SlWRKY42* improve salt-alkali tolerance in tomato (Liu *et al.* 2025). Based on these findings, we propose that the interactions between MiCOL14B-GQ/JH and MiRZFP34, MiPP2C39A, or MiWRKYs may directly or indirectly enhance stress tolerance in plants. Nevertheless, the precise molecular mechanisms underlying these interactions require further investigation.

5. Conclusion

Based on our findings, we propose a model (Fig. 10) in which *MiCOL14B*-GQ and *MiCOL14B*-JH have opposing roles in regulating flowering but convergent roles in stress tolerance in mango. In flowering regulation, MiCOL14B-GQ acts as a repressor by downregulating *MiFT1a1* and *MiFT1b* through direct suppression of their promoter activity. In contrast, MiCOL14B-JH functions as an activator of these floral integrators. This functional divergence is attributed to differences in their structural domain composition. In stress responses, both proteins interact with partners such as MiRZFP34, and MiWRKYs, however, only MiCOL14B-JH was found to interact with MiPP2C39A. These interactions enhance plant tolerance to salt and drought stress by elevating proline content and SOD activity while reducing H_2O_2 and MDA levels, thereby enhancing the plant's antioxidant capacity. Thus, the regulation of *MiCOL14B*-GQ and *MiCOL14B*-JH expression represents a key mechanism influencing both mango flowering time and tolerance to adverse conditions like salt and drought. These findings have potential applications for improving the agronomic traits of mango and other crops. The functional divergence in flowering induced by differences in structural domains also provides a theoretical basis for future studies focusing on knocking out or introducing specific domains to alter gene functions. Future studies should further investigate the specific molecular mechanisms underlying *MiCOL14B*-GQ and *MiCOL14B*-JH in regulating flowering and stress resistance, and explore their potential applications in mango breeding on the basis of these mechanisms.

Acknowledgements

This research was supported by the National Natural Science Foundation of China (32360726), the Guangxi Key Technologies R&D Program, China (Guikenong AB241484007) and the CARSGIT-Guangxi Mango Industry Project, China (nycytxgxcxtd-2021-06-02).

Declaration of competing interest

The authors declare that they have no conflict of interest.

Declaration of generative AI and AI-assisted technologies in the writing process

During the preparation of this manuscript, the authors used DeepSeek-V3.1 to assist in improving the clarity and readability of the language. All content generated was carefully reviewed and revised by the authors as necessary, and the authors take full responsibility for the final content of the article.

Appendices associated with this paper are available at https://doi.org/10.1016/j.jia.2026.01.012

References

Bajpai A, Muthukumar M, Bajpai Y, Anand S, Ahmad I, Das A. 2017. Salinity induced growth, physiological and gene expression responses in polyembryonic mango cultivars. *Green Farming*, **8**, 1076–1080.

Blazquez M A, Green R, Nilsson O, Sussman M R, Weigel D. 1998. Gibberellins promote flowering of *Arabidopsis* by activating the *LEAFY* promoter. *Plant Cell*, **10**, 791–800.

Böhlenius H, Huang T, Charbonnel-Campaa L, Brunner A M, Jansson S, Strauss S H, Nilsson O. 2006. *CO*/*FT* regulatory module controls timing of flowering and seasonal growth cessation in trees. *Science*, **312**, 1040–1043.

Cai X W, Xiao L, Nie X M, Hou Q D, Wen S L, Yang K, Wen X P. 2025. HpFBH3 transactivates *HpCO7* via binding to the E-boxes in the promoter and may accelerate flower formation in pitaya. *Journal of Integrative Agriculture*, **24**, 575–593.

Cao X, Xie H, Song M, Lu J, Ma P, Huang B, Wang M, Tian Y, Chen F, Peng J, Lang Z, Li G, Zhu J K. 2023. Cut-dip-budding delivery system enables genetic modifications in plants without tissue culture. *The Innovation*, **4**, 100345.

Chen J, Chen J Y, Wang J N, Kuang J F, Shan W, Lu W J. 2012. Molecular characterization and expression profiles of *MaCOL1*, a *CONSTANS-like* gene in banana fruit. *Gene*, **496**, 110–117.

Chen J H. 2002. Guire mango no.82 — a fine mid-ripening mango variety. *Guangxi Tropical Agriculture*, **1**, 16–29. (in Chinese)

Chen P, Zhi F, Li X, Shen W, Yan M, He J, Bao C, Fan T, Zhou S, Ma F, Guan Q. 2022. Zinc-finger protein MdBBX7/MdCOL9, a target of MdMIEL1 E3 ligase, confers drought tolerance in apple. *Plant Physiology*, **188**, 540–559.

Chen S Q, Luo C, Liu Y, Liang R Z, Huang X, Guo Y H, Li R Y, Huang C T, Wang Z, He X H. 2023. Lack of the CCT domain changes the ability of mango *MiCOL14A* to resist salt and drought stress in Arabidopsis. *Plant Science*, **335**, 111826.

Chen X S. 2000. Preliminary report on the introduction and trial planting of Jinhuan mango. *Guangxi Tropical Crops Science & Technology*, **1**, 11–12. (in Chinese)

Corbesier L, Vincent C, Jang S, Fornara F, Fan Q Z, Searle I, Giakountis A, Farrona S, Gissot L, Turnbull C, Coupland G. 2007. FT protein movement contributes to long-distance signaling in floral induction of Arabidopsis. *Science*, **316**, 1030–1033.

Cui Z K, Tu Z H, Yang L C, Li W, Wu J P, Li H G. 2023. Overexpression of the *Liriodendron chinense CONSTANS* gene in Arabidopsis causes earlier flowering under long-day conditions. *Plant Growth Regulation*, **100**, 577–591.

Deivasigamani P, Vijayakumar R M, Balakrishnan S, Arulmozhiselvan K, Sivakumar R. 2018. Effect of salt stress on morphological characters of mango rootstocks. *International Journal of Chemical Studies*, **6**, 387–389.

Du J C, Zhu X, He K R, Kui M Y, Zhang J P, Han X, Fu Q T, Jiang Y J, Hu Y R. 2023. CONSTANS interacts with and antagonizes ABF transcription factors during salt stress under long-day conditions. *Plant Physiology*, **193**, 1675–1694.

Endo M, Tanigawa Y, Murakami T, Araki T, Nagatani A. 2013. PHYTOCHROME-DEPENDENT LATE-FLOWERING accelerates flowering through physical interactions with phytochrome B and CONSTANS. *Proceedings of the National Academy of Sciences of the United States of America*, **110**, 18017–18022.

Feng X, Wu X L, Wu H L, Li Y, Zhou B J, Jiang y, Zhang S L, Wei J L, Su S C, Hou Z X. 2025. Short-photoperiod induces floral induction involving carbohydrate metabolism and regulation by *VcCO3* in greenhouse blueberry. *Plant, Cell & Environment*, **48**, 2145–2161.

Gangappa S N, Crocco C D, Johansson H, Datta S, Hettiarachchi C, Holm M, Botto J F. 2013. The *Arabidopsis* B-BOX protein BBX25 interacts with HY5, negatively regulating *BBX22* expression to suppress seedling photomorphogenesis. *The Plant Cell*, **25**, 1243–1257.

González A M, Vander Schoor J K, Fang C, Kong F, Wu J, Weller J L, Santalla M. 2021. Ancient relaxation of an obligate short-day requirement in common bean through loss of *CONSTANS-like* gene function. *Current Biology*, **31**, 1643–1652.

Gou J L, Sang X L, Liu L Q, Cao J S, Liu Y, Ren C, Zhang Z X, Jue D W, Shi S Y. 2025. Genome-wide identification and functional analysis of the longan *CONSTANS* (*CO*) family. *BMC Plant Biology*, **25**, 418.

Guo Y H, Luo C, Liu Y, Liang R Z, Yu H X, Lu X X, Mo X, Chen S Q, He X H. 2022. Isolation and functional analysis of two *CONSTANS-like 1* genes from mango. *Plant Physiology and Biochemistry*, **172**, 125–135.

Huang J H. Ma W H. Liang G L. Zhang L Y. Wang W X. Cai Z J. Wen S X. 2010. Effects of low temperatures on sexual reproduction of 'Tainong 1' mango (*Mangifera indica*). *Scientia Horticulturae*, **126**, 109–119.

Lagercrantz U, Axelsson T. 2000. Rapid evolution of the family of *CONSTANS-LIKE* genes in plants. *Molecular Biology and Evolution*, **17**, 1499–1507.

Lee J, Lee I. 2010. Regulation and function of *SOC1*, a flowering pathway integrator. *Journal of Experimental Botany*, **61**, 2247–2254.

Lei X, Tan B, Liu Z, Wu J, Lv J, Gao C. 2021. *ThCOL2* improves the salt stress tolerance of *Tamarix hispida*. *Frontiers in Plant Science*, **12**, 653791.

Li J J, Lu T T, Mo W J, Yu H X, Li K J, Huang X, Fan Z Y, He X H, Luo C. 2024. Functional characterization of *MiFT*s implicated in early flowering and stress resistances of mango. *International Journal of Biological Macromolecules*, **280**, 135669.

Li R Y, Luo C, Zhong J J, Liu Y, Wen H B, Xu F, He Z X, Huang C T, He X H. 2025. Functional identification of mango *MiGID1A* and *MiGID1B* genes confers early flowering and stress tolerance. *Plant Science*, **355**, 112468.

Liang R Z, Luo C, Liu Y, Hu W L, Guo Y H, Yu H X, Lu T T, Chen S Q, Zhang X J, He X H. 2023. Overexpression of two *CONSTANS-like 2* (*MiCOL2*) genes from mango delays flowering and enhances tolerance to abiotic stress in transgenic Arabidopsis. *Plant Science*, **327**, 111541.

Liu C Y, Zhang Q Q, Zhu H, Cai C M, Li S. 2021. Characterization of Mungbean *CONSTANS-LIKE* genes and functional analysis of *CONSTANS-LIKE 2* in the regulation of flowering time in Arabidopsis. *Frontiers in Plant Science*, **12**, 608603.

Liu L, Ding Q, Liu J, Yang C, Chen H, Zhang S, Zhu J, Wang D. 2020a. *Brassica napus COL* transcription factor *BnCOL2* negatively affects the tolerance of transgenic *Arabidopsis* to drought stress. *Environmental and Experimental Botany*, **178**, 104171.

Liu X, Shang C, Duan P, Yang J, Wang J, Sui D, Chen G, Li X, Li G, Hu S, Hu X. 2025. The *SlWRKY42-SlMYC2* module synergistically enhances tomato saline-alkali tolerance by activating the jasmonic acid signaling and spermidine biosynthesis pathway. *Journal of Integrative Plant Biology*, **67**, 1254–1273.

Liu Y, Luo C, Guo Y H, Liang R Z, Yu H X, Chen S Q, Lu T T, Mo X, He X H. 2022a. Isolation and functional characterization of two *CONSTANS-like 16* (*MiCOL16*) genes from mango. *International Journal of Molecular Sciences*, **23**, 3075.

Liu Y, Luo C, Lan M Y, Guo Y H, Li R Y, Liang R Z, Chen S Q, Zhong J J, Li B J, Xie F F, Chen C B, He X H. 2024. *MiCOL6*, *MiCOL7A* and *MiCOL7B* isolated from mango regulate flowering and stress response in transgenic Arabidopsis. *Physiologia Plantarum*, **176**, e14242.

Liu Y, Luo C, Liang R Z, Lan M Y, Yu H X, Guo Y H, Chen S Q, Lu T T, Mo X, He X H. 2022b. Genome-Wide identification of the mango *CONSTANS* (*CO*) family and functional analysis of two *MiCOL9* genes in transgenic Arabidopsis. *Frontiers in Plant Science*, **13**, 1028987.

Liu Y, Luo C, Zhang X J, Lu X X, Yu H X, Xie X J, Fan Z Y, Mo X, He X H. 2020b. Overexpression of the mango *MiCO* gene delayed flowering time in transgenic *Arabidopsis*. *Plant Cell, Tissue and Organ Culture*, **143**, 219–228.

Livak K J, Schmittgen T D. 2001. Analysis of relative gene expression data using real-time quantitative PCR and the $2^{-\Delta\Delta Ct}$ method. *Methods*, **25**, 402–408.

Lu J, Sun J J, Jiang A Q, Bai M J, Fan C G, Liu J Y, Ning G G, Wang C Q, Wang C Q. 2020. Alternate expression of *CONSTANS-LIKE 4* in short days and *CONSTANS* in long days facilitates day-neutral response in *Rosa chinensis*. *Journal of Experimental Botany*, **71**, 4057–4068.

Lu T T, Wei R Y, Mo W J, Li K J, Yu H X, Wei H Y, He X H, Luo C. 2023. Overexpression of mango *MiRZFP34* confers early flowering and stress tolerance in transgenic *Arabidopsis*. *Scientia Horticulturae*, **312**, 111868.

Luo C, He X H, Chen H, Hu Y, Ou S J. 2013. Molecular cloning and expression analysis of four actin genes (*MiACT*) from mango. *Biologia Plantarum*, **57**, 238–244.

Lv X C, Zeng X L, Hu H M, Chen L X, Zhang F, Liu R, Liu Y, Zhou X L, Wang C S, Wu Z, Kim C H, He Y H, Du J M. 2021. Structural insights into the multivalent binding of the *Arabidopsis FLOWERING LOCUS T* promoter by the CO-NF-Y master transcription factor complex. *The Plant Cell*, **33**, 1182–1195.

Ma H J, Pei J L, Zhuo J, Tang Q Y, Hou D, Lin X C. 2024. The *CONSTANS-Like* Gene *PeCOL13* regulates flowering through intron-retained alternative splicing in *Phyllostachys edulis*. *International Journal of Biological Macromolecules*, **274**, 133393.

Ma Z X, Jia Y, Min Y W, Fang X, Yan H D, Ma Q, Cai R H. 2025. Maize *ZmWRKY71* gene positively regulates drought tolerance through reactive oxygen species homeostasis. *Plant Physiology and Biochemistry*, **219**, 109399.

Mutasa G E, Hedden P. 2009. Gibberellin as a factor in floral regulatory networks. *Journal of Experimental Botany*, **60**, 1979–1989.

Nemoto Y, Nonoue Y, Yano M, Izawa T. 2016. *Hd1*, a *CONSTANS* ortholog in rice, functions as an *Ehd1* repressor through interaction with monocot-specific CCT-domain protein Ghd7. *Plant Journal*, **86**, 221–233.

Niu F, Rehmani M S, Yan J. 2024. Multilayered regulation and implication of flowering time in plants. *Plant Physiology and Biochemistry*, **213**, 108842.

Okamuro J K, Szeto W, Lotys-Prass C, Jofuku K D. 1997. Photo and hormonal control of meristem identity in the *Arabidopsis* flower mutants *apetala2* and *apetala1*. *Plant Cell*, **9**, 37–47.

Onouchi H, Igeño M I, Périlleux C, Graves K, Coupland G. 2000. Mutagenesis of plants overexpressing *CONSTANS* demonstrates novel interactions among *Arabidopsis* flowering-time genes. *Plant Cell*, **12**, 885–900.

Putterill J, Robson F, Lee K, Simon R, Coupland G. 1995. The *CONSTANS* gene of *Arabidopsis* promotes flowering and encodes a protein showing similarities to zinc finger transcription factors. *Cell*, **80**, 847–857.

Robson F, Costa M M R, Hepworth S R, Vizir I, Piñeiro M, Reeves P H, Putterill J, Coupland G. 2001. Functional importance of conserved domains in the flowering-time gene *CONSTANS* demonstrated by analysis of mutant alleles and transgenic plants. *Plant Journal*. **28**, 619–631.

Ruan Y, Wang M, Xiao M, Liu B, Zhou J, Yang Y, Huang Y. 2024. Identification and function analysis of *PP2C* gene family shows that *BnaA2.PP2C73* negatively regulates drought and salt stress responses in *Brassica napus* L. *Industrial Crops and Products*, **214**, 118568.

Shim J S, Kubota A, Imaizumi T. 2017. Circadian clock and photoperiodic flowering in *Arabidopsis*: CONSTANS is a hub for signal integration. *Plant Physiology*, **173**, 5–15.

Srikanth A, Schmid M. 2011. Regulation of flowering time: All roads lead to Rome. *Cellular and Molecular Life Sciences*, **68**, 2013–2037.

Tamaki S, Matsuo S, Wong H L, Yokoi S, Shimamoto K. 2007. Hd3a protein is a mobile flowering signal in rice. *Science*, **316**, 1033–1036.

Tiwari S B, Shen Y, Chang H C, Hou Y L, Harris A, Ma S F, McPartland M, Hymus G J, Adam L, Marion C, Belachew A, Repetti P P, Reuber T L, Ratcliffe O J. 2010. The flowering time regulator *CONSTANS* is recruited to the *FLOWERING LOCUS T* promoter via a unique *cis*-element. *New Phytologist*, **187**, 57–66.

Wang Q Q, Liu W, Leung C C, Tarté D A, Gendron J M. 2024. Plants distinguish different photoperiods to independently control seasonal flowering and growth. *Science*, **383**, 9196.

Wen X X, Zhong Z Z, Xu P, Yang Q Q, Wang Y P, Liu L, Wu Z Z, Wu Y W, Zhang Y X, Liu Q N, Zhou Z P, Peng Z Q, He Y Q, Cheng S H, Cao L Y, Zhan X D, Wu W X. 2024. *OsCOL5* suppresses heading through modulation of *Ghd7* and *Ehd2*, enhancing rice yield. *Theoretical and Applied Genetics*, **137**, 162.

Wigge P A, Kim M C, Jaeger K E, Busch W, Schmid M, Lohmann J U, Weigel D. 2005. Integration of spatial and temporal information during floral induction in *Arabidopsis*. *Science*, **309**, 1056–1059.

Wu G, Park M Y, Conway S R, Wang J W, Weigel D, Poethig R S. 2009. The sequential action of miR156 and miR172 regulates developmental timing in *Arabidopsis*. *Cell*, **138**, 750–759.

Wullschleger S D, Weston D J. 2012. Modeling the molecular and climatic controls on flowering. *New Phytologist*, **194**, 599–601.

Xu C J, Shan J M, Liu T M, Wang Q, Ji Y J, Zhang Y T, Wang M Y, Xia N, Zhao L. 2023. *CONSTANS-LIKE 1a* positively regulates salt and drought tolerance in soybean. *Plant Physiology*, **191**, 2427–2446.

Yang W B, Zhou C C, Guo Y T, Niu S H, El-Kassaby Y A, Li W. 2024. Genome-wide identification of the *Pinus tabuliformis CONSTANS-like* gene family and their potential roles in reproductive cone development. *International Journal of Biological Macromolecules*, **254**, 127621.

Yano M, Katayose Y, Ashikari M, Yamanouchi U, Monna L, Fuse T, Baba T, Yamamoto K, Umehara Y, Nagamura Y, Sasaki T. 2000. *Hd1*, a major photoperiod sensitivity quantitative trait locus in rice, is closely related to the *Arabidopsis* flowering time gene *CONSTANS*. *Plant Cell*, **12**, 2473–2483.

Zhang Z P, Shi W J, Gu J W, Song S X, Xiao M, Yao J C, Liu Y C, Jiang J Z, Miao M M. 2024. Short day promotes gall swelling by a *CONSTANS-FLOWERING LOCUS T* pathway in *Zizania latifolia*. *The Plant Journal*, **120**, 1014–1031.

Zhao Y Z, Xu J H, Xu X Y, Liu H, Chang Q X, Xu L, Liang Z S. 2025. Genome-wide identification of *CONSTANS-like* (*COL*) gene family and the potential function of *ApCOL08* under salt stress in *Andrographis paniculata*. *International Journal of Molecular Sciences*, **26**, 724.